Article

Cancer Cell

# Tumoral Immune Cell Exploitation in Colorectal Cancer Metastases Can Be Targeted Effectively by Anti-CCR5 Therapy in Cancer Patients

## Graphical Abstract

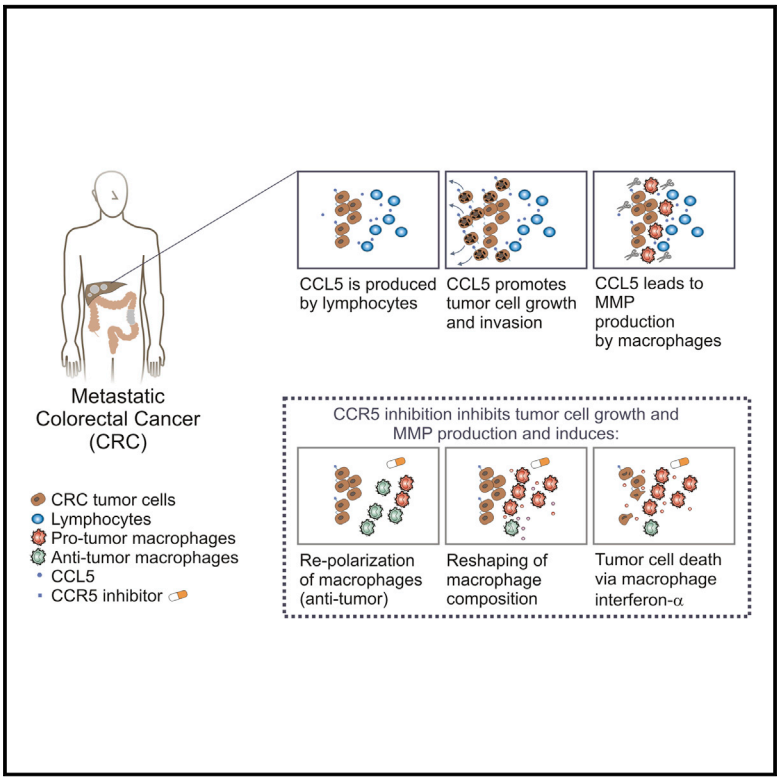


## Authors

Niels Halama, Inka Zoernig, Anna Berthel, ..., Niels Grabe, Christine S. Falk, Dirk Jaeger

## Correspondence

niels.halama@nct-heidelberg.de

## In Brief

Halama et al. show that T cells at invasive margins of human colorectal cancer (CRC) liver metastases produce CCL5, which has tumor-promoting effects on tumor cells and tumor-associated macrophages. CCR5 blockade mitigates the tumor-promoting microenvironment and leads to clinical responses in CRC patients.

## Highlights

- CCL5 is produced by $CD4^+$ and $CD8^+$ T lymphocytes in colorectal cancer liver metastases
- CCL5's natural receptor CCR5 is found on tumor cells, lymphocytes and myeloid cells
- Inhibition of CCR5 leads to repolarization of tumor-associated macrophages
- CCR5 inhibition leads to objective clinical responses in colorectal cancer patients

Halama et al., 2016, Cancer Cell *29*, 587–601
April 11, 2016 
http://dx.doi.org/10.1016/j.ccell.2016.03.005

CellPress

Cancer Cell
Article

# Tumoral Immune Cell Exploitation in Colorectal Cancer Metastases Can Be Targeted Effectively by Anti-CCR5 Therapy in Cancer Patients

Niels Halama,[1,2,3,*] Inka Zoernig,[1] Anna Berthel,[1,2] Christoph Kahlert,[4,6] Fee Klupp,[4] Meggy Suarez-Carmona,[1] Thomas Suetterlin,[1,2] Karsten Brand,[5] Juergen Krauss,[1] Felix Lasitschka,[5] Tina Lerchl,[1,2] Claudia Luckner-Minden,[1] Alexis Ulrich,[4] Moritz Koch,[6] Juergen Weitz,[6] Martin Schneider,[4] Markus W. Buechler,[4] Laurence Zitvogel,[7] Thomas Herrmann,[8] Axel Benner,[9] Christina Kunz,[9] Stephan Luecke,[9] Christoph Springfeld,[1] Niels Grabe,[1,2] Christine S. Falk,[10,11] and Dirk Jaeger[1,2,11]

[1]Department of Medical Oncology, National Center for Tumor Diseases, University Hospital Heidelberg, 69120 Heidelberg, Germany
[2]Tissue Imaging and Analysis Center, National Center for Tumor Diseases, BIOQUANT, University of Heidelberg, 69120 Heidelberg, Germany
[3]Institute for Immunology
[4]Department of Surgery
[5]Institute for Pathology
University Hospital Heidelberg, 69120 Heidelberg, Germany
[6]Department of Surgery, University Hospital Dresden, 01307 Dresden, Germany
[7]INSERM U1015, Institut Gustave Roussy (IGR), 94805 Villejuif, France
[8]Department of Internal Medicine I, Klinikum Idar-Oberstein, 55743 Idar Oberstein, Germany
[9]Division of Biostatistics, German Cancer Research Center (DKFZ), 69120 Heidelberg, Germany
[10]Institute of Transplant Immunology, Integrated Research and Treatment Center Transplantation, Hannover Medical School, 30625 Hannover, Germany
[11]Co-senior author
*Correspondence: niels.halama@nct-heidelberg.de
http://dx.doi.org/10.1016/j.ccell.2016.03.005

## SUMMARY

**The immune response influences the clinical course of colorectal cancer (CRC). Analyzing the invasive margin of human CRC liver metastases, we identified a mechanism of immune cell exploitation by tumor cells. While two distinct subsets of myeloid cells induce an influx of T cells into the invasive margin via CXCL9/CXCL10, CCL5 is produced by these T cells and stimulates pro-tumoral effects via CCR5. CCR5 blockade in patient-derived functional in vitro organotypic culture models showed a macrophage repolarization with anti-tumoral effects. These anti-tumoral effects were then confirmed in a phase I trial with a CCR5 antagonist in patients with liver metastases of advanced refractory CRC. Mitigation of tumor-promoting inflammation within the tumor tissue and objective tumor responses in CRC were observed.**

## INTRODUCTION

Cancer progression utilizes an evolving crosstalk between different cells, involving especially cancer cells and immune cells (Coussens et al., 2013). Cancer patients typically die due to tumor progression and metastatic burden (Sethi and Kang, 2011). In colorectal cancer (CRC), irresectable (hepatic) metastases herald a poor prognosis with a median overall survival of 24 months (Sethi and Kang, 2011; Van Cutsem et al., 2009). Treatment approaches such as PD-1/PD-L1 blockade (Melero

### Significance

We demonstrate a tumor-promoting role for $CD4^+$ and $CD8^+$ T lymphocytes in metastatic colorectal cancer that directly elicit proliferation and production of pro-tumorigenic inflammatory cytokines mediated by CCL5-CCR5. Tumor promotion is induced by enhanced migratory properties of tumor cells and pro-metastatic factors produced by tumor-associated macrophages. This mechanism can be targeted effectively in human cancer patients by blocking CCR5, which also leads to anti-tumoral repolarization of macrophages. This work reveals a pro-tumorigenic mechanism involving components of the immune system that are exploited effectively in metastases to promote tumor growth and invasion. Translation into a clinical trial confirmed the therapeutic efficacy of CCR5 blockade, especially in mitigating this pro-tumor inflammatory microenvironment through effects on both tumor cells and tumor-associated macrophages.

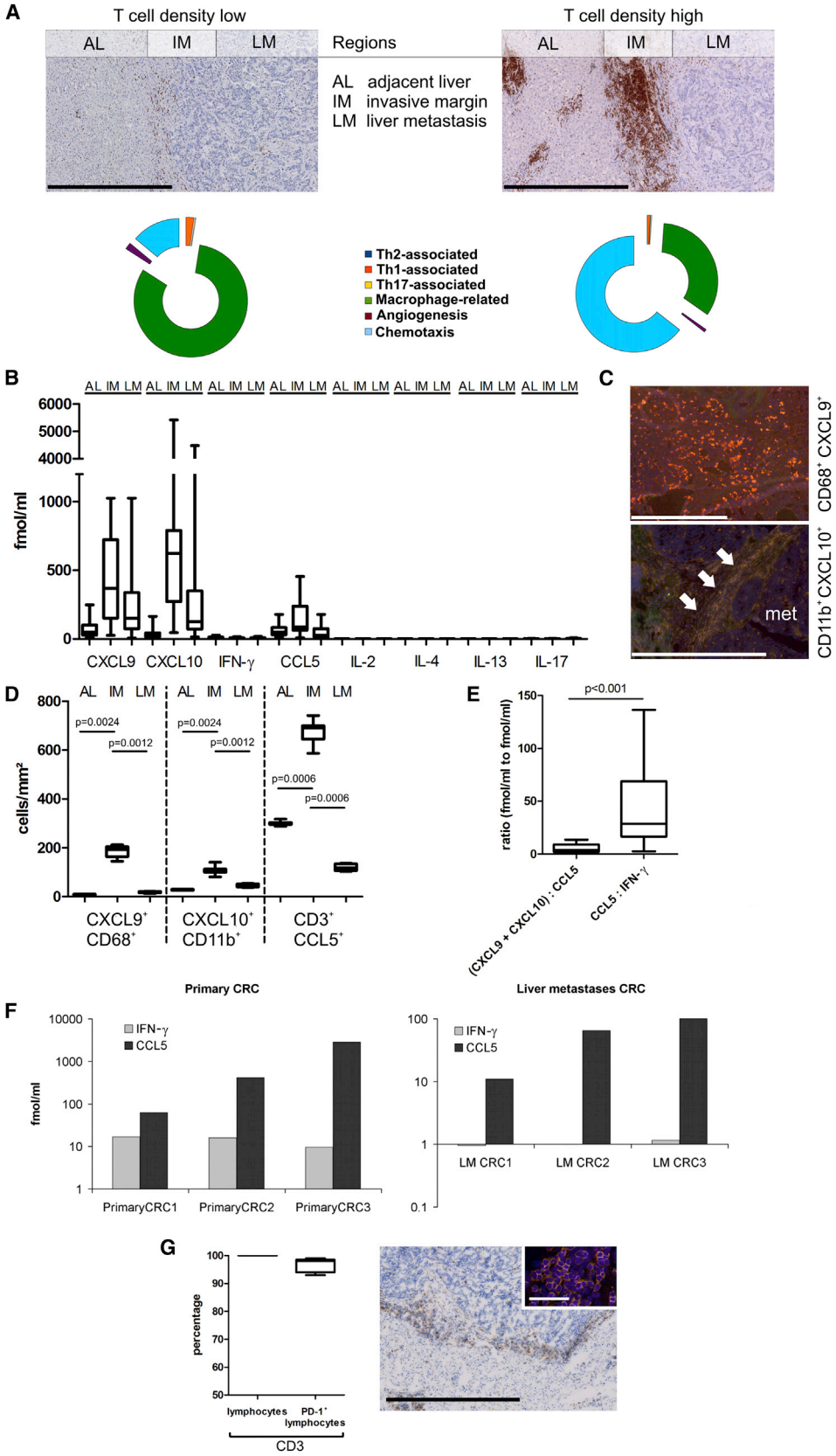


(legend on next page)

et al., 2007; Topalian et al., 2012) or chemokine modulation (Acharyya et al., 2012; Stewart and Smyth, 2009) successfully modify interactions between the immune system and cancer toward rejection or, at least, suppression of progression (Vanneman and Dranoff, 2012). While the presence of specific subtypes of immune cells is beneficial for the patient, cancer cells can also alter the immune microenvironment and the function of immune cells, leading to immunosuppression and immune evasion (Fridman et al., 2012; Gabrilovich et al., 2012). But how does the local immunological microenvironment in liver metastases of CRC patients contribute to tumor progression? The invasive margin of CRC metastases harbors a variety of immune cells that are specific for this compartment, i.e., large conglomerates of T cells and monocytes (Halama et al., 2009a). We have identified this invasive margin as an important compartment for shaping prognosis and response to chemotherapy in patients with CRC liver metastases, apart from the central parts of the metastasis (Halama et al., 2011b; Keim et al., 2012). The absence of natural killer cells in the metastases underlines the specific differential regulation of immune cells in these compartments (Halama et al., 2011a). Large numbers of tumor-associated macrophages form a significant cellular fraction in this microenvironment, but the intricate functional interconnection between the myeloid compartment and effector lymphocytes is unclear in human metastatic CRC (Affara et al., 2014; DeNardo et al., 2011).

Our in-depth analysis of the microenvironment in CRC liver metastases allowed us to differentiate a network of tumor cells and immune cells (and their cytokines) that exploits the CCL5-CCR5 axis within the microenvironment (Oppermann, 2004; Velasco-Velazquez et al., 2012). Here, we investigated and characterized the effects of blocking the CCL5-CCR5 axis.

## RESULTS

### The Invasive Margin Is an Immunologically Distinct Microenvironment Dominated by Chemokines and Macrophage-Related Cytokines

In line with our previous work, we here saw that T cells cluster specifically at the invasive margin (Figure 1A) (Halama et al., 2011b). To understand the underlying cytokine microenvironment, we determined concentrations of cytokines and chemokines in 60 liver metastases, after dissecting invasive margins, the liver metastases, and adjacent liver tissues (Figures 1A, 1B, S1A, and S1B).

In general, no relevant Th1 (interleukin-2 [IL-2], interferon-γ (IFN-γ]), Th2 (IL-4, -5, -13), and Th17 (IL-17)-specific cytokine signature was present in any of the analyzed samples (Figure 1A). IL-10 concentrations were below biological significance in all analyzed samples (see also Lee et al., 2012; Pardoll, 2012). Cytokines showed a distinct pattern at the invasive margin (Figures 1B and 1C) compared with the center of the metastatic lesion and the adjacent normal liver, revealing a unique microenvironment in this region. Together with macrophage-related cytokines, the chemokines CXCL9, CXCL10, and CCL5 were significantly increased at the invasive margin (Figure 1B) in all analyzed samples. Both CXCL9 and CXCL10 were produced by specialized subpopulations of either $CD68^+$ or $CD11b^+$ cells (Figure 1C), with both chemokines being positively correlated with (effector) T cell density as published previously (Halama et al., 2011a; Mlecnik et al., 2009). Immunofluorescent double staining revealed a specific $CD68^+$ monocyte subpopulation producing CXCL9 almost exclusively in the invasive margin (Figures 1C, 1D, and S1C) without CD68/CXCL10 double-positive cells (data not shown). Conversely, a $CD11b^+$ subpopulation at the invasive margin produced CXCL10 (Figures 1C, 1D, and S1D). CXCL9- or CXCL10-producing cells are not tumor cells as evidenced by double staining and laser-assisted microdissection with mutational profiling (Figures S1E–S1G). Both CXCL9 and CXCL10 are produced by myeloid cells and are known to induce lymphocyte migration via CXCR3 (Figure S1H). In contrast, CCL5 is produced exclusively by $CD3^+$ T lymphocytes at the invasive margin (Figure 1D). The combined CXCL9 and CXCL10 concentrations were generally higher than CCL5 concentrations (Figure 1E); however, the ratio of CCL5 to IFN-γ was even significantly higher, demonstrating an immunological imbalance due to the lack of IFN-γ (Figure 1E). While CCL5 concentrations remained almost at the same level between primary tumors and metastases, IFN-γ declined below levels of biological significance in metastases (Figure 1F), indicating a functionally altered situation (“exhaustion”) with increased CCL5 production of the infiltrating $CD3^+$ lymphocytes. The clinical success of PD-1/PD-L1 blockade prompted us to investigate PD-1 expression by lymphocytes in these tissue sections. Indeed, 98% of $CD3^+$ lymphocytes in the resection specimens were positive for PD-1 (Figure 1G), and the location of these PD-1-positive lymphocytes converged with $CD68^+$ PD-L1-expressing cells, whereas tumor cells were PD-L1 negative at the invasive margin (Figure S1I) as previously described (Kuang et al., 2009).

**Figure 1. The Invasive Margin Is a Microenvironment with Distinct Cellular and Cytokine Compositions**

(A) CD3ε immunostaining showing diverse T cell densities at the invasive margin of two exemplary liver metastases from two patients with CRC. The pie charts show the observed classifications (e.g., Th2, etc.) of the corresponding cytokine concentrations measured in the invasive margin, where 100% is the sum of all concentrations of all measured cytokines. Scale bar, 800 μm.

(B) Overview of relevant cytokine and chemokine concentrations across different regions (n = 60 each).

(C) Myeloid subsets that produce either CXCL9 or CXCL10 in the invasive margin. Scale bars, 800 μm (upper panel) and 200 μm (lower panel, arrows indicate invasive margin).

(D) Cell densities of CXCL9-, CXCL10-, or CCL5-positive cells at different regions.

(E) Ratios of the CXCR3 axis (CXCL9 and CXCL10 concentrations) compared with CCL5 concentrations and ratios of CCL5 and IFN-γ at the invasive margin (n = 60).

(F) IFN-γ and CCL5 concentrations from three primary tumors and metastases.

(G) Percentage of PD-1-positive $CD3^+$ lymphocytes in the tumor microenvironment and an example of a colorectal cancer liver metastasis immunostained for PD-1 (scale bar, 800 μm). The inset shows a representative virtual double stain (yellow stain indicates $CD3^+PD1^+$ double-positive lymphocytes; scale bar, 50 μm). See also Figure S1.

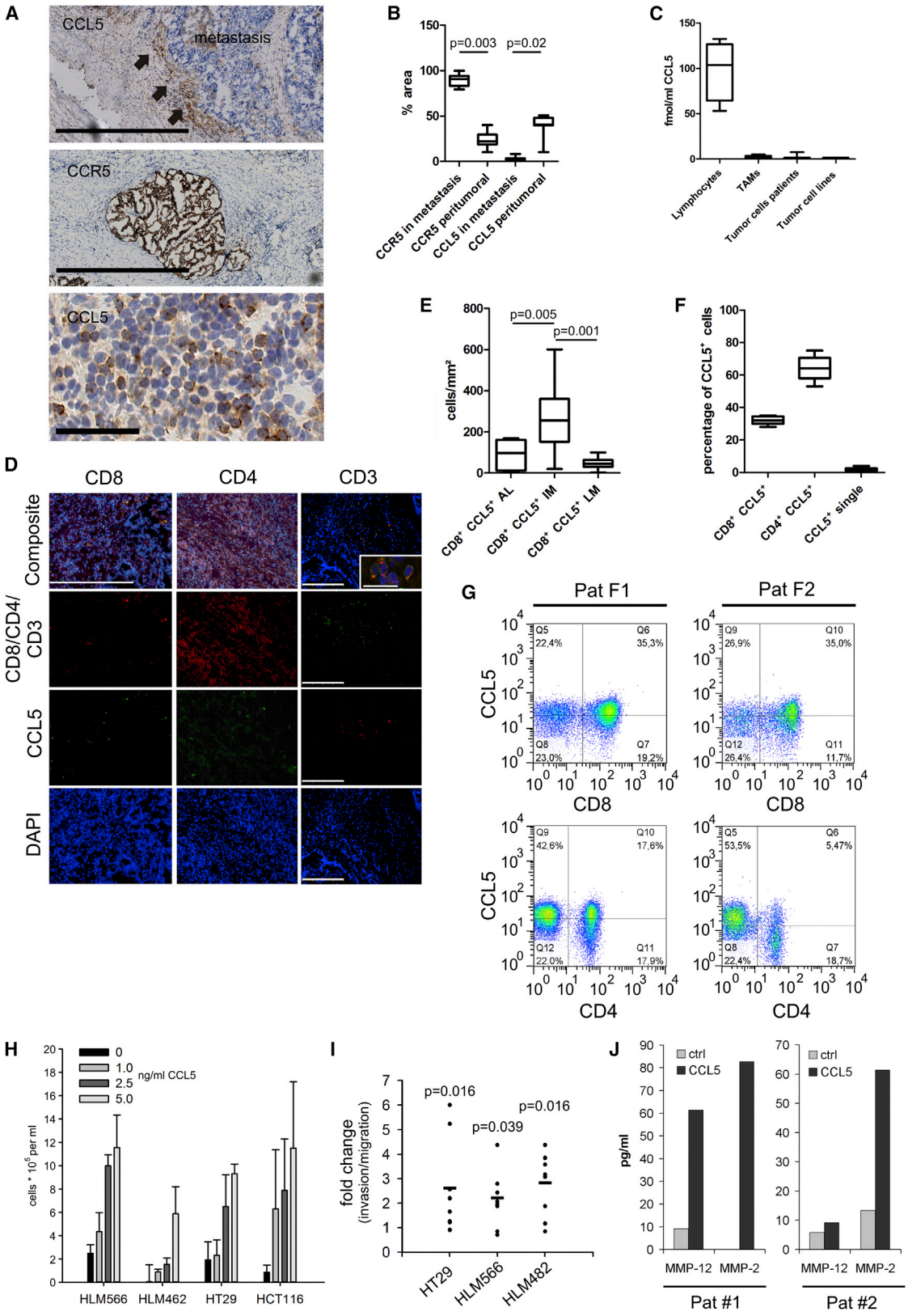


**Figure 2. CD4⁺ and CD8⁺ T Cells Alone Produce CCL5, which Leads to Tumor Growth and Invasion**

(A) Representative distribution pattern of CCL5 at the invasive margin of the liver metastasis (upper panel; black arrows indicate CCL5 staining in the stroma; scale bar, 1 mm) and representative CCR5 distribution pattern shows a strong presence on the tumor cell compartment in a liver metastasis nodule surrounded by

*(legend continued on next page)*

### T Cell-Derived CCL5 Has Pleiotropic Tumor-Promoting Effects on Tumor Cells and Tumor-Associated Macrophages

While CCL5 was produced by T cells localized mainly at the invasive margin and peritumoral stroma of metastases, the receptor CCR5 was dominantly expressed by metastatic tumor cells (Figures 2A–2C) and to a lower extent by lymphocytes and myeloid cells (Figure S2A). CCR5 is typically absent on tumor cells in the primary tumor in early stages of CRC (Musha et al., 2005). In our samples from CRC liver metastases, all samples were found to have CCR5 on tumor cells. As T lymphocytes were identified as the unique relevant source of CCL5 (Figure 2C), immunofluorescence, confocal microscopy, virtual triple staining (Figure S2B), and fluorescence-activated cell sorting analyses further revealed that $CD3^+CD4^+$ and $CD3^+CD8^+$ T cells (and practically these cells alone, Figures S2C–S2E) produce CCL5 in the microenvironment (Figures 2D–2G), which in turn has potent tumor-promoting properties with respect to proliferation (Figure 2H), invasive tumor cell behavior (Figure 2I), and increased production of matrix metalloproteinases by tumor-associated macrophages (Figures 2J and S2F). The spatial proximity between CCL5 and markers of epithelial to mesenchymal transition (EMT) was noted in all samples, and consequently substantial effects of CCR5 inhibition on key molecules of EMT were identified (Figures S2G and S2H). The other known CCL5 receptors CCR1 and CCR3 were not found on tumor cells but only on immune cells (data not shown).

### Anti-tumor Effects of CCR5 Inhibition Are Mediated through Macrophage Repolarization via STAT3 Regulation in Organotypic Explant Models

With the identification of CCL5 as a T lymphocyte-derived chemokine, affecting both tumor cells and tumor-associated macrophages (TAMs), we decided to test the effects of CCR5 blockade using maraviroc, a highly selective, well-tolerated, and approved CCR5 inhibitor that was originally developed for HIV patients as viral entry blocking inhibitor (Dorr et al., 2005). As there are no mouse models recapitulating the complex immunological microenvironment in advanced-stage pre-treated metastatic CRC, we functionally tested the effects of CCR5 blockade using human tumor explant models (Ellis and Fidler, 2010). Fresh tissue samples contain the complete tumor microenvironment and display good stability of cytokine and chemokine production as well as histological composition in short-term culture (Figures 3A and S3A–S3C). Maraviroc was applied to several tumor tissue explants from different advanced CRC patients with liver metastases. Histological analysis revealed that maraviroc led to morphologically overt tumor cell death in the explants (Figures 3B and S3D) and a pattern of alterations of cytokine and chemokine levels. Reductions of inflammatory cytokines such as macrophage migration inhibitory factor (MIF), CXCL8, IL-1 receptor antagonist (IL1RA), and vascular endothelial growth factor (VEGF) within the tumor microenvironment occurred, while leaving the adjacent liver unchanged (Figure 3C). In the presence of maraviroc, $CD11b^+$ cells were identified as the major source of IFN-$\alpha$2 and IFN-$\gamma$ (Figures 3D and 3E). IFN-$\alpha$2 and IFN-$\gamma$ levels were dynamically increased by maraviroc as well as the numbers of IFN-$\alpha2^+$ cells within the tissue (Figures 3E and 3F). Inhibition of INF-$\alpha$2 abrogated the induction of morphologically overt tumor cell death (Figures 3G and S3E). In line with these observations, CCL5 had a negative effect on the production of IFN-$\alpha$2 (Figure 3H).

To test the hypothesis that macrophages are required for the tumor cell death-inducing effects of CCR5 blockade, we used clodronate liposomes to deplete $CD163^+$ TAMs. Clodronate alone did not show anti-tumoral effects in our 48- to 72-hr explant model despite the specific reduction of $CD163^+$ cell numbers and reduced macrophage-associated cytokines (Figures S4A–S4C). However, combining clodronate with CCR5 inhibition abrogated the immediate tumor cell death-inducing effects of CCR5 inhibition, confirming the role of macrophages in this process (Figures 4A, 4B, and S4D).

Further experiments showed that IFN-$\gamma$ induced stromal $CD163^+$ macrophage cell death and leads to a reconfiguration of the myeloid cell compartment (Figures S4E and S4F), which could be abrogated by blocking IFN-$\gamma$ or IFN-$\gamma$ receptor 1, respectively (Figure 4C). In addition, inhibition of macrophage-derived reactive oxygen species by L-NAME (L-$N^G$-nitroarginine methyl ester) could partially block the anti-tumoral effects of CCR5 inhibition (Figure S4G).

In TAMs treated with CCL5, increased levels of SOCS3 and PIAS3 were abrogated by CCR5 inhibition, leading to increased STAT3 levels (Figure 4D) commonly linked to an M1 polarization state (Qin et al., 2012). Protein phosphorylation patterns in these TAMs showed an activation of Akt and ERK1/2 pathways in response to elevated STAT3 and an increased phosphorylation of glycogen synthase kinase-3 (GSK3) and c-JUN (Figures 4E and S4H). The simultaneous increase of type I IFN levels is

stroma (middle panel; scale bar, 1 mm). The lower panel shows $CCL5^+$ lymphocytes at the invasive margin (scale bar, 100 μm). Representative images from all analyzed samples of liver metastases from CRC.

(B) CCR5 or CCL5 positively stained areas for different compartments as quantified using whole-slide image analysis.

(C) CCL5 production of different cells in in vitro culture. Lymphocytes and tumor-associated macrophages were isolated from ascites of CRC patients.

(D) Immunofluorescent staining of the microenvironment for indicated molecules. DAPI (blue) is used as counterstain; scale bars represent 400 μm for CD8/CD4 and 200 μm for CD3. Representative images from all analyzed samples. Inset: higher magnification confocal image of CD3/CCL5 (scale bar, 20 μm).

(E) $CCL5^+CD8^+/CD4^+$ cell densities in different regions, quantified with whole-slide image analysis. AL, adjacent liver; IM, invasive margin; LM, liver metastases.

(F) Quantification of $CCL5^+$, $CCL5^+CD8^+$, and $CCL5^+CD4^+$ cells using virtual triple stain on serial sections of the invasive margin (n = 25).

(G) Flow cytometry analysis of $CD4^+CCL5^+$ and $CD8^+CCL5^+$ cells, gated on $CD3^+$ cells, of tissue specimens from the invasive margin of two patients.

(H) Growth effects of varying concentrations of CCL5 on different tumor cell lines treated for 4 days. Error bars denote SEM.

(I) Matrigel invasion assay of different tumor cell lines with CCL5 added to the lower chamber relative to the respective control without CCL5 averaged from three quantifications. Wilcoxon signed-rank test. Horizontal bars represent average.

(J) Matrix metalloproteinase (MMP) production in tumor-associated macrophages isolated from ascites of two patients with or without CCL5 treatment (5 ng/ml for 24 hr).

See also Figure S2.

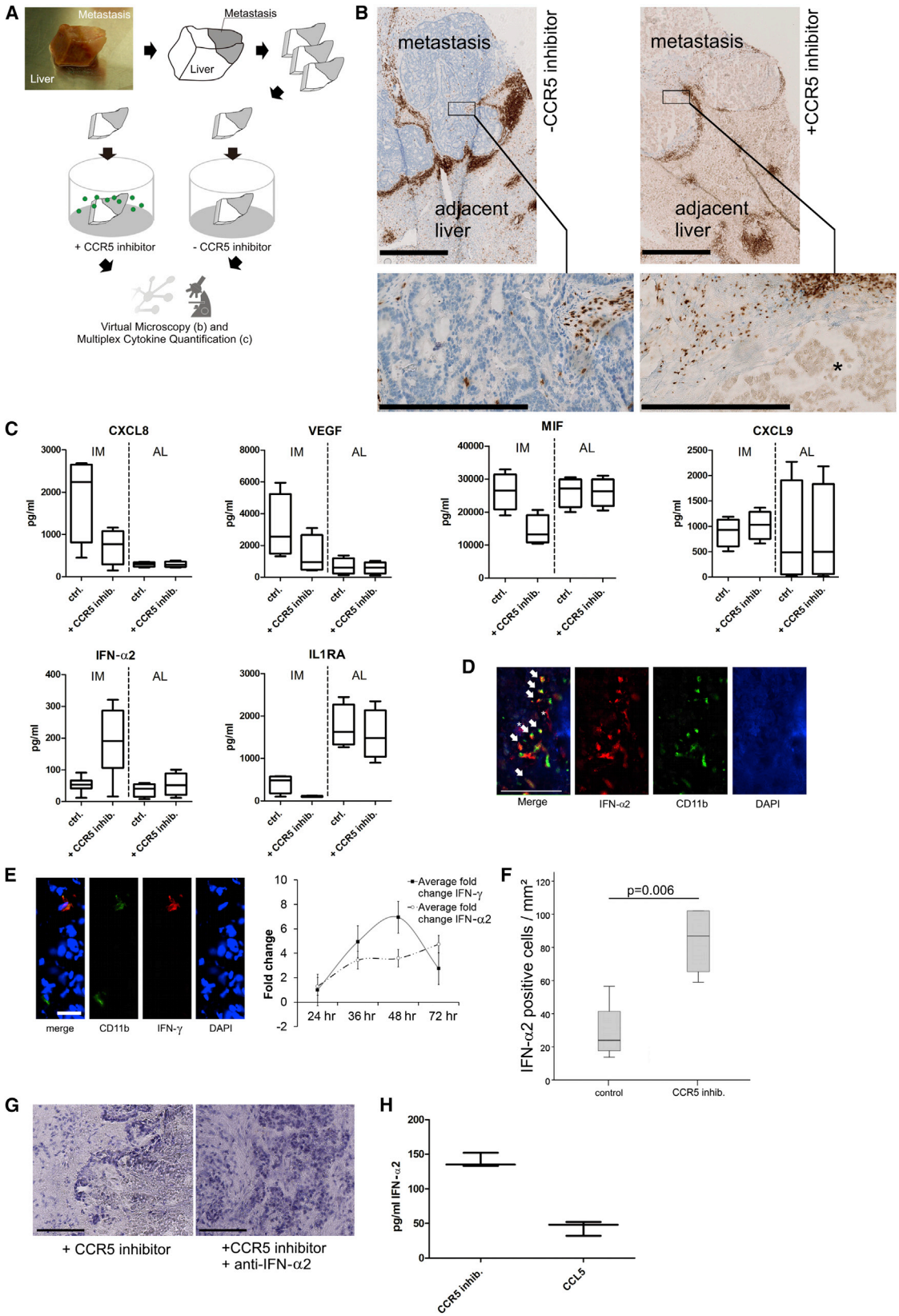


(legend on next page)

indicative of an antiviral response pattern induced in these macrophages (Trinchieri, 2010).

To confirm that these effects are due to CCL5/CCR5 inhibition and are not related to the chemical compound maraviroc, we evaluated a CCL5 neutralizing antibody and a CCR5 blocking antibody. Both showed similar functional effects to maraviroc regarding secretion of chemokines, cytokines, and growth factors (Figure 4F). Indirect reduction of CCL5 through neutralization of CXCL9/10 or through clodronate liposomes to deplete CXCL9/10-producing myeloid cells in the explant model system did not recapitulate the effect of anti-CCR5 due to slow migration of localized T cells out of the invasive margin and subsequent moderately decreased levels of CCL5 and no significant effect on IFN-α2 (Figures 4G and S4I, and data not shown).

Conversely, addition of CCL5 to CRC explant tissue induced a reverse effect on cytokines, thereby fostering a tumor-promoting microenvironment and corroborating a specific effect of the CCR5/CCL5 axis independently of the mode of interference (Figure 4H and data not shown).

### CCR5 Blockade in CRC Patients Leads to the Expected Mitigation of the Tumor-Promoting Microenvironment and Objective Clinical Responses

As maraviroc does not have significant side effects in its current use in HIV infections and the explant model data suggested beneficial effects of CCR5 blockade in metastatic CRC, we decided to launch a pilot clinical trial (MARACON) in patients with advanced-stage metastatic colorectal cancer who are refractory to standard chemotherapy, including regorafenib (Tables 1, 2, and S1) (Abel et al., 2008; Reshef et al., 2012). All patients on the trial were shown to express CCR5 histologically in CRC cells, and no patient had a homozygous CCR5 delta32 variant.

Patients received 300 mg of maraviroc twice daily with a pre-treatment biopsy and a second biopsy of the same liver metastasis after treatment for 8–10 days (Figure 5A). Observed clinical effects include induction of central tumor necrosis (Figure 5B) and a partial remission of lung metastases (Figures 5C and S5A). In a patient with malignant pleural effusions, the reduction of MIF and hepatocyte growth factor (HGF) seen in the explant models was recapitulated within the effusion (Figure S5B), highlighting the systemic effects of maraviroc. On a histological level, all tumor samples showed reduced proliferation (as evidenced by Ki67 staining, Figure S5C) and increased tumor cell death as evidenced by morphology (Figure 5D), while the morphology of the adjacent normal liver was unchanged (Figure 5D). Moreover, the effects on the microenvironment induced by maraviroc as seen in the short-term explant models could also be observed in the patient biopsies. Marked reductions in key cytokines and growth factors promoting tumor growth, chemotherapy resistance, or angiogenesis were seen in most clinical samples (Figure 5E). In addition, the density of $CD8^+$ (and other) infiltrating cells at the invasive margin was unchanged or minimally increased in five of six analyzed patient samples (Figure S5D) with increased numbers of IFN-α2-positive cells under treatment with maraviroc (Figure S5E).

All patients had received previously all of the standard-of-care treatments (including regorafenib for some patients, Tables 1 and 2) with an average of 4.3 lines of previous treatment. Nevertheless, maraviroc treatment was very well tolerated. The most commonly observed treatment-related adverse events were mild elevation of liver enzymes (Table 3). Median overall survival was 5.06 months for the core cohort (95% confidence interval, 3.06 months to infinity). From the 11 patients of the core cohort, five decided to be re-exposed to chemotherapy after participation in the trial. Patients were allowed to receive maraviroc in combination with chemotherapy, as the biopsies from the trial had shown anti-tumoral effects at the tissue level. Of these five patients, three had objective partial responses (60%, Figures 5F and 5G), one patient had stable disease, and one was not evaluable, so that a tumor control rate of 80% was achieved (Table 4). Overall survival in this subgroup, including patient 4 whose tumor had a *BRAF* mutation and who had had no objective response to any previous treatment, showed a median of 7.69 months (95% confidence interval, from 6.18 months to infinity). The data from the extension cohort showed a median overall survival of 6.94 months (6.91, 6.94, 16.08 months) and both cohorts together showed a 7.32-month overall survival (95% confidence interval, from 6.91 months to infinity). Taken together, the MARACON trial confirmed the absence of significant side effects for maraviroc treatment in previously treated metastatic CRC patients. Finally, partial responses were achieved in patients with previously refractory disease.

## DISCUSSION

The invasive margin of CRC liver metastases is an immunological microenvironment of its own dimensions. Our data clearly show that this environment induces migration of T lymphocytes into the invasive margin following a distinct chemokine gradient. Infiltrating T lymphocytes exert tumor-stimulating effects via their own production of CCL5. We here report an exploitive

**Figure 3. Tumor Explant Models Show Mitigation of the Tumor-Promoting Cytokines and Selective Tumor Cell Death upon Treatment with CCR5 Inhibitor**

(A) Schematic overview of processing of the tumor explant material. See Supplemental Experimental Procedures for details.

(B) Histological alterations within the explant model, showing morphologically disintegrated tumor epithelium (asterisk) and intact stroma with infiltrating T cells (CD3ε staining shown). Scale bar, 1 mm.

(C) Cytokine alterations within the explant model after 36 hr. Data from five different patients for the invasive margin (IM) and from three for the adjacent liver (AL).

(D) Immunofluorescent staining of tumor explant as indicated. Arrows indicate double-positive cells and asterisk indicates vessel. Scale bar, 100 μm.

(E) Immunofluorescent staining of tumor explants after treatment with maraviroc (4 nM, 48 hr) (left; scale bar, 25 μm) and fold change in concentrations of IFN-γ and IFN-α2 over time under CCR5 inhibition in tumor explant models (n = 5; error bars denote SEM).

(F) Number of IFN-α2-positive cells/$mm^2$ in explant models before and after maraviroc treatment (quantification of positively stained cells).

(G) Histomorphological effects of IFN-α2 blocking antibodies (pre-treatment 1 hr prior to CCR5 inhibition). Scale bar, 100 μm.

(H) CCL5 effects on IFN-α2 levels in tumor explants (boxplot, n = 3).

See also Figure S3.

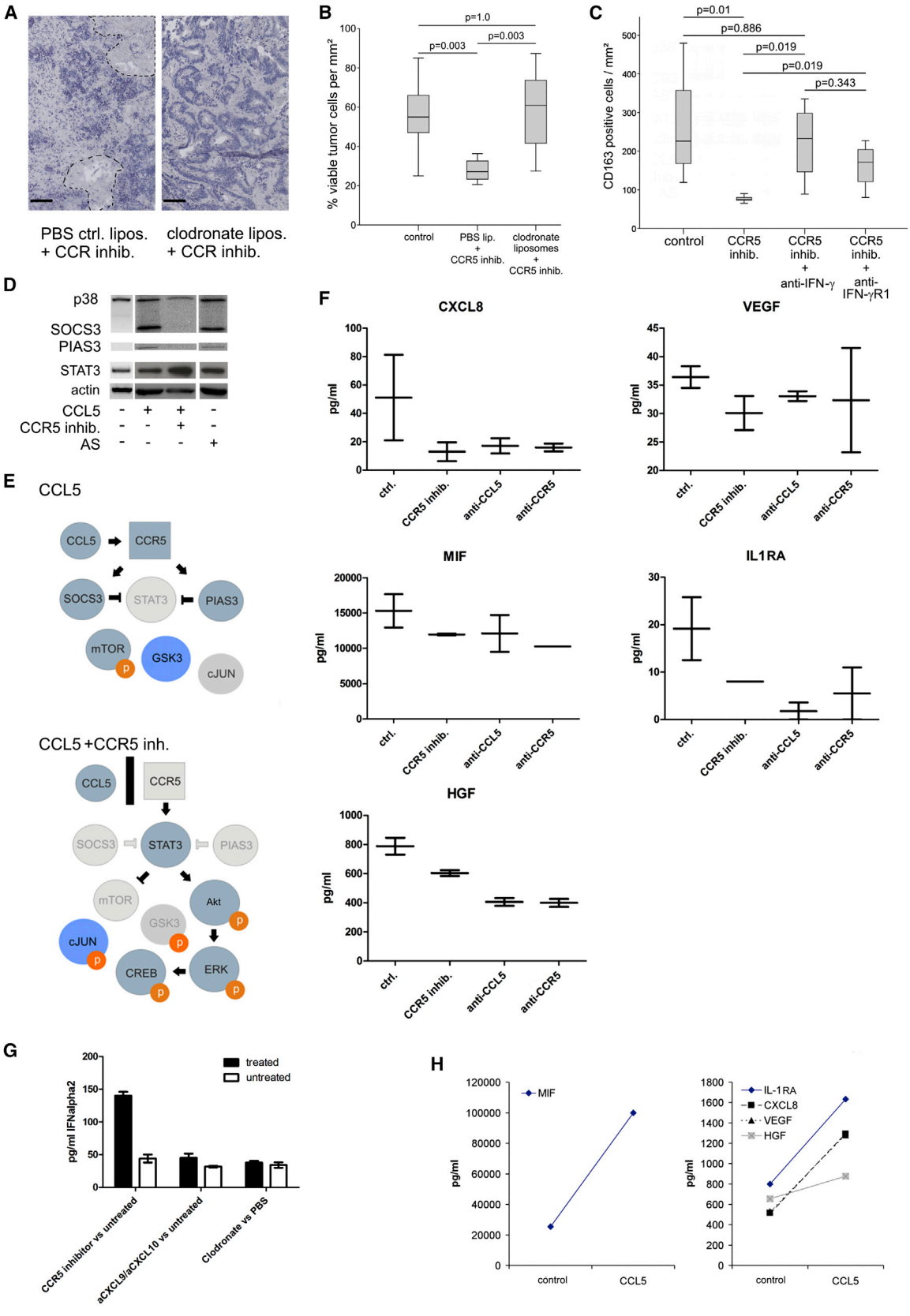


(legend on next page)

**Table 1. Patient Characteristics**

| Patients | T | N | M | Grade | Age (years) | Gender | *KRAS* | *BRAF* | No. of Previous Therapies |
|---|---|---|---|---|---|---|---|---|---|
| Core cohort | | | | | | | | | |
| 1 | 3 | 2 | 1 | 2 | 62 | male | mut | WT | 4[a] |
| 2 | 4 | 2 | 1 | 2 | 68 | female | WT | WT | 5 |
| 3 | 3 | 2 | 1 | 3 | 33[b] | female | WT | WT | 3 |
| 4 | 3 | 2 | 1 | 2 | 32[b] | male | WT | mut[c] | 2 |
| 5 | 3 | 2 | 1 | 3 | 60 | male | mut[d] | WT | 4 |
| 6 | 3 | 2 | 1 | 2 | 69 | male | mut[d] | WT | 6[a] |
| 7 | 4 | 0 | 1 | 3 | 65 | male | WT | WT | 3 |
| 8 | 3 | 1 | 1 | 3 | 62[b] | male | mut[d] | WT | 4 |
| 9 | 3 | 1 | 1 | 2 | 68 | male | mut | WT | 6 |
| 10 | 3 | 1 | 1 | 1 | 71 | male | WT | WT | 3 |
| 11 | 4 | 2 | 1 | 2 | 66 | female | WT | WT | 7 |
| Extension cohort | | | | | | | | | |
| 12 | 3 | 0 | 1 | 2 | 62 | male | mut | WT | 4 |
| 13 | 4 | 1 | 1 | 2 | 65 | female | mut[d] | WT | 6[a] |
| 14 | 3 | 1 | 1 | 2 | 58 | male | mut[d] | WT | 3[a] |

See also Table S1.
[a]Including regorafenib.
[b]Microsatellite-stable tumor.
[c]*BRAF* mutation V600E.
[d]Codon 12 (mut: *KRAS* mutation without further specifics).

immunoresistance involving both CD4 and CD8 T cells (DeNardo and Coussens, 2007). The microenvironment in liver metastases of CRC shows no Th1, Th2, or Th17 milieu but instead is optimized for tumor-promoting inflammation involving chemokines and growth factors such as VEGF, HGF, and MIF. It is well perceived that CXCL9 and CXCL10 produced by myeloid cells attract T lymphocytes via their chemokine receptor CXCR3 (Lee et al., 2012). As a consequence of this CXCR3-mediated migration, tumor-infiltrating lymphocytes at the invasive margin of CRC liver lesions deliver CCL5, which in turn supports tumor growth and tumor cell spread by pro-tumoral polarization of macrophages. Our findings highlight (1) an immunosuppressive landscape, (2) a potential tumor-protective mechanism of CRC metastases, and (3) the tumor-promoting properties of specific immune cell subsets. The CCL5-CCR5 loop represents a mechanism tumor cells can utilize for their growth advantage, by creating a spatial "division" to exploit the host's immune cell anti-tumor efforts. It is known that Th1 cells can induce PD-L1 expression via IFN-γ as an immunoevasive mechanism (Pardoll, 2012), but here T cells are even further exploited: CCL5 produced by immune cells alone, not by the tumor cells, supports tumor growth and dissemination by modulation of macrophages with production of matrix metalloproteinases or induction of EMT in tumor cells (Barashi et al., 2013; Liou et al., 2013). The spatial convergence of tumor cells, chemokine-producing myeloid cells, CCL5-producing lymphocytes, and TAMs generates an effective pro-tumorigenic inflammatory environment (Coussens et al., 2013).

The effects of CCR5 blockade on the tissue level show induction of tumor cell death and a specific pattern of cytokine and

**Figure 4. CCR5 Inhibition Leads to Anti-tumor Repolarization of Macrophages**

(A) Effects on tissue integrity induced by macrophage inhibition and depletion (via liposomal clodronate) prior to CCR5 inhibition. Dashed lines indicate areas of necrosis/dead tumor cells. Hemalaun staining. Scale bar, 100 μm.

(B) Effects of 1 hr pre-treatment of explant models (n = 5) with clodronate liposomes (or control PBS liposomes) to induce macrophage depletion followed by CCR5 inhibition.

(C) $CD163^+$ macrophage densities with CCR5 inhibition, CCR5 inhibition, and IFN-γ neutralizing antibodies or CCR5 inhibition and IFN-γ receptor 1 blocking antibodies.

(D) Western blot results of macrophage polarization markers from tumor-associated macrophages (TAM), untreated (medium alone), and treated with CCL5, CCR5 inhibitor, or ascites supernatant (AS).

(E) Schematic signaling effects of CCR5 inhibition on TAMs with modulation of STAT3, Akt, and GSK3 leading to IFN production. Pointed arrows indicate activation, T shaped arrows indicate inhibition, and arrows do not necessarily indicate direct interaction of two proteins. Gray molecules are inactive (all others are active); orange circles indicate phosphorylation. Upper panel shows effects of CCL5 alone without CCR5 inhibition; lower panel shows effects of CCL5 plus CCR5 inhibition (indicated by vertical black bar).

(F) Cytokine alterations induced by different CCR5/CCL5 inhibitory molecules (tumor explants, n = 3, boxplots). ctrl., untreated reference.

(G) Effects of anti-CXCL9/anti-CXCL10 treatment or clodronate treatment compared to CCR5 inhibitor effects on IFN-α2 levels in tumor explant tissues (n = 3; error bars denote SEM).

(H) CCL5-induced effects on cytokines in a tumor tissue explant.

See also Figure S4.

| Table 2. Extended Patient Characteristics | |
|---|---|
| Core Trial Population | n = 11 |
| Patients with ≥4 previous therapies (%) | 63.64 |
| Patients with <18 months from diagnosis of metastases to trial (%) | 36.36 |
| *BRAF* mutation (%) | 9.09 |
| Prior regorafenib treatment (%) | 18.18 |
| Extension Population | n = 3 |
| Patients with ≥4 previous therapies (%) | 66.67 |
| Patients with <18 months from diagnosis of metastases to trial (%) | 0 |
| *BRAF* mutation (%) | 0 |
| Prior regorafenib treatment (%) | 66.67 |

chemokine modulation, found in the explant model as well as in the tumor biopsies from the clinical trial. Macrophages are the key for these anti-tumoral effects: production of IFNs and reactive oxygen species form the main axis of tumor cell death. These macrophages are already present in the tumor microenvironment, and CCR5 blockade induces a phenotypic shift, which is mediated via STAT3/SOCS3 in TAMs, referred to as a switch from an M2 to an M1 phenotype. Together with the concomitant modulation of GSK3 and c-JUN, it can be interpreted here as the activation of an ''antiviral response pattern'' in macrophages (Qian and Pollard, 2012; Qin et al., 2012). This ''repolarization'' also reduces levels of $CD163^+$ cells and, thereby, is not only a macrophage repolarization therapy but also reshapes myeloid cell composition in the microenvironment. The demonstration of this macrophage phenotype switch induced by CCR5 inhibition in human cancer patients elucidates the therapeutic anti-tumoral stimulation of innate immune cells. During CCR5 inhibition, the pre-existing CXCL10 and CXCL9 gradients and $CD8^+$ T cell densities remain constant or even increase. Potentially, with the influx of new effector cells the deleterious effects of CCL5 could be shifted toward the beneficial effects of IFN-$\alpha$2 and IFN-$\gamma$ (Hervas-Stubbs et al., 2011). Reduction of immunosuppression via MIF, angiogenesis via VEGF, and chemotherapy resistance via CXCL8 and increased IFN levels could possibly contribute to this anti-tumoral effect and also add to the momentum of CCR5 inhibition combined with chemotherapy (Hwang et al., 2011; Sistigu et al., 2014; Yan et al., 2006).

How do these observations fit into previous findings that a high T cell density at the tumor site is associated with a better clinical outcome (Fridman et al., 2012; Galon et al., 2006)? Our observations indicate a shift in the balances between IFN and CCL5 production by lymphocytes and CCR5 expression in the metastatic stage of the disease, i.e., a changing immune contexture (Dunn et al., 2004; Fridman et al., 2012; Klein, 2009). T cells have different roles in primary tumors versus metastases. While tumor cell killing in the early stages of the tumor (i.e., non-metastatic primary tumor) is possible via IFN-$\gamma$ without interventions such as radiation or chemotherapy, in the metastatic stage the CCL5/CCR5 axis is exploited by the tumor (Klein, 2009; Zitvogel et al., 2008). Due to ethical reasons practically all patients with irresectable CRC liver metastases receive palliative chemotherapy, and published data show reinvigoration of T cells (with, e.g., increased IFN production) and a shift in the balance toward a less immunosuppressive environment so that immune effector cells and chemotherapy-induced tumor cell death (immunogenic cell death) can work synergistically (Zitvogel et al., 2008). Therefore, a higher density of T cells is most likely beneficial because larger numbers of reinvigorated T cells open the door for anti-tumoral effects by direct killing or through cytokine production. The CCR5-CCL5 axis in metastatic disease is another complexity of the scenario whereby the tumor protects itself from immune responses and escapes tumor surveillance even in a situation with a favorable T cell infiltration. Patients with irresectable metastatic CRC die of tumor progression even with a favorable T cell infiltration at the metastatic site, and the CCL5-CCR5 axis is exploited in this progression.

Clinical data suggest that the observed effects of CCL5/CCR5 are not limited to the liver metastases, but are a systemic feature. The local heterogeneous presence of multiple layers of immune subversion in cancers depends not only on the individual tissue, treatment, tumor type, or the difference between primary tumor and metastatic lesion, but also makes it necessary to integrate temporal tissue dynamics, as identified in our study.

The concordance of the fully human organotypic tumor explant models and the findings in the biopsies from patients of the MARACON trial is encouraging. Although it is a simple model with a rather straightforward approach, the observed short-term effects were prospectively validated in the patients of the trial.

Survival data from the MARACON trial is not conclusive due to the limited number of patients and the much more unfavorable clinical features of these patients compared with typical patient cohorts on fourth- or fifth-line therapy (Grothey et al., 2013). Looking at the trial data, it is nevertheless clear that the subsequent objective treatment responses are very encouraging. Historically the objective response rates in patients on or after the third line of chemotherapy are around 5%–10% (Nielsen et al., 2014). No large datasets exist on patients on or after fourth-line therapy, but objective responses were generally not observed and chemotherapy is only applied for symptom control (Arkenau et al., 2009). This is in contrast to our result of a high response rate in this advanced situation.

Taken together, CCR5 blockade may seem counterintuitive but showed clinical effects with regression of metastatic disease and alterations of the tumor microenvironment without significant side effects (Gonzalez-Martin et al., 2012). The clinical objective response rate in subsequent chemotherapies is promising and shows the potential for combination therapy: macrophages providing enhancing type I IFN for chemotherapy efficacy (Coussens et al., 2013; DeNardo et al., 2011; Hales et al., 2010; Sistigu et al., 2014). Thus, activation of anti-tumoral polarization in macrophages via CCR5 blockade appears to be a promising approach and needs to be evaluated further scientifically and clinically.

## EXPERIMENTAL PROCEDURES

### Patient Material

All material mentioned herein was obtained after approval by the medical ethics committee of the University of Heidelberg, and written consent was obtained from all patients prior to analysis. All samples were obtained

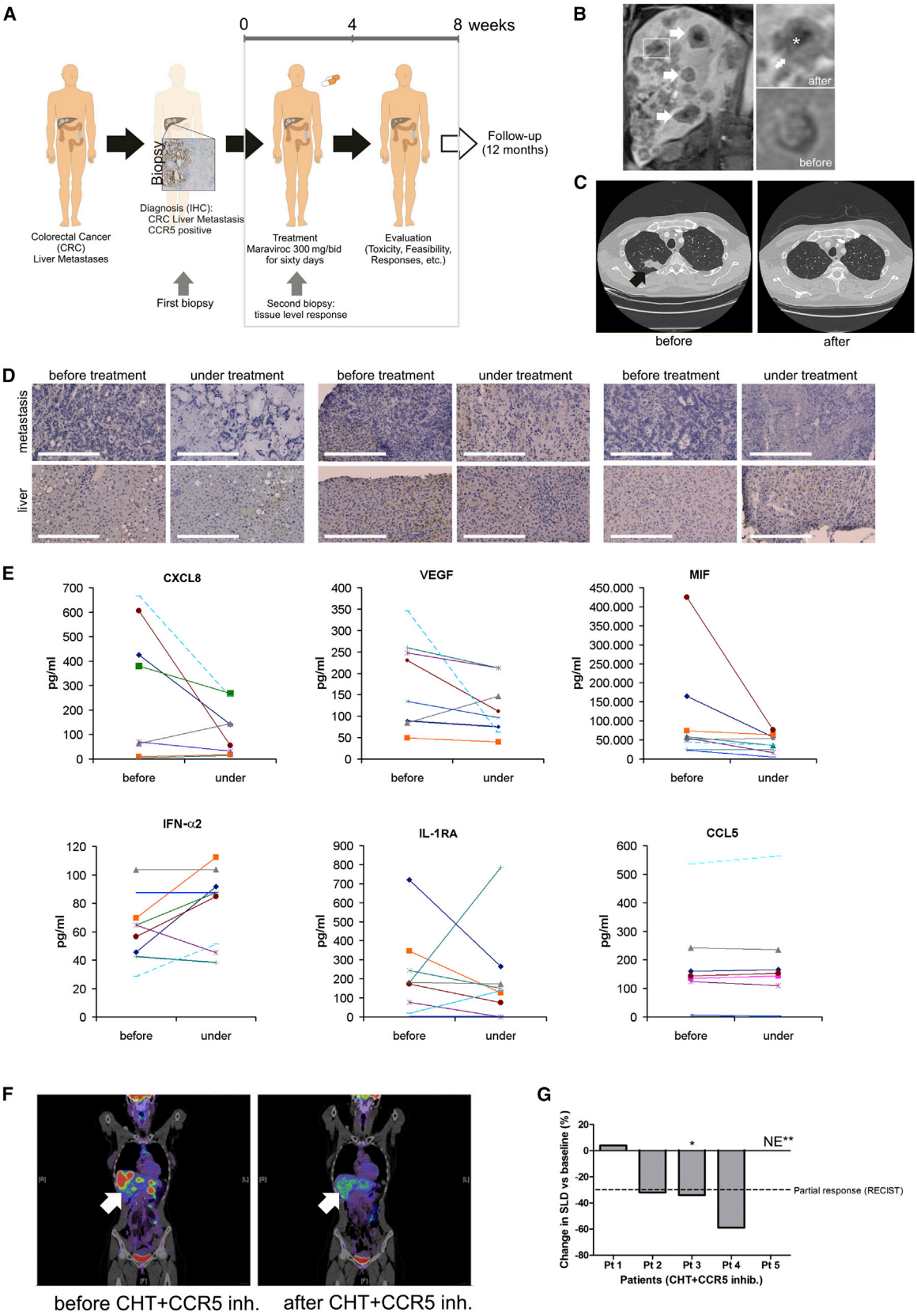


(legend on next page)

from the Institute of Pathology and the Department of Surgery at the University of Heidelberg. Histopathological and clinical findings were scored according to the International Union Against Cancer (UICC) TNM staging system.

A set of 60 samples from patients with liver metastases of CRC was analyzed to generate the cytokine and chemokine data. These were frozen specimens of surgically resected liver metastases from CRC patients (without previous chemotherapy).

In this first cohort (70.69% males), age ranged from 35 to 79 with a mean age of 62.8 years. All of these samples were from liver metastases, and the corresponding primary tumors had the following properties: 56.25% were metachrone, 18.42% T1, 63.16% T2, 18.42% T3, 54.05% N0, 24.32% N1, 21.62% N2, 75% G2, and 25% G3.

In addition, 30 paraffin-embedded samples from 20 primary CRC tumors and ten samples from hepatic metastases were analyzed. For the primary tumors five samples were UICC stage I, five stage II, five stage III, and five stage IV. Of all tumor and metastases samples 10% of the tumors were well differentiated (G1), 70% tumors were of intermediate differentiation (G2), and poor differentiation (G3) was seen in 20% of tumors, according to standard morphological features. Tumor samples were typed for microsatellite instability using BAT25, BAT26, and CAT25 as described earlier (Findeisen et al., 2005) and no microsatellite instability was found. Pathological reports were available for all tissues, and no samples from patients with inflammatory bowel disease were included in this analysis.

The second liver metastases cohort consisted of resected material from the invasive margin that was used directly for organotypic model experiments. These patients had undergone heavy treatment with at least one chemotherapeutic regimen consisting of either FOLFOX or FOLFIRI. In patients with metachrone liver metastases, adjuvant chemotherapy had been given.

### Cell Preparation, Cell Culture, and Proliferation Assays

Commercially available tumor cell lines or primary cells extracted from ascites or blood were used in the experiments. Characterized cell lines were maintained according to their recommendations in culture media containing RPMI 1640 (PAA Laboratories), 10% fetal bovine serum (FBS Superior; Biochrom), 1% glutamine (PAA), 1% penicillin/streptomycin (PAA), 1% non-essential amino acids (PAA), and 1% HEPES (PAA). Primary cell culture media contained DMEM (high glucose with L-glutamine; PAA), 1% penicillin/streptomycin (PAA), 1% non-essential amino acids (PAA), and 1% HEPES (PAA). Tumor explant models were cultured in MEM (10× MEM; Gibco) and 1% glutamine (PAA).

### Multiplex Protein Quantification

Multiplex protein quantification was performed on dissected tissues as described previously (Halama et al., 2013; Zhou et al., 2008). For detection of chemokines, cytokines, and matrix metalloproteinases in tissue and cell samples, lysates were prepared according to the manufacturer's instructions (Bio-Rad). Molecular concentrations were calculated based on the molecular mass of each cytokine.

### Immunohistochemistry and Immunofluorescence

Tissue specimens were immunohistochemically analyzed for the presence and spatial distribution of immune cell markers (e.g., CD3, CD8) or specific other (surface) antigens (e.g., CCR5, CCL5). Tissue sections (4 μm) were prepared from either formalin-fixed, paraffin-embedded tissue or cryo-conserved specimens (7 μm). Cryosections were fixed with either 4% paraformaldehyde (Sigma-Aldrich) or 33% acetone in methanol prior stainings. The complete staining procedure was carried out on a BOND Max (Leica).

### Whole-Slide Immune Cell Quantification

The number of stained immune cells was counted using a computerized image analysis system consisting of an NDP Nanozoomer (Hamamatsu Photonics) attached to a personal computer. Complete microscopic images of full tissue sections were automatically obtained (virtual microscopy) and the average cell density across the measured region was used for analysis. Cell counts were generated with a specifically developed software program (VIS software suite; Visiopharm) across a given region of interest (on average 10 $mm^2$, with up to 40 $mm^2$) as reported previously (Halama et al., 2009b, 2010, 2011b). All evaluations were visually checked for consistency.

### Primary Cell Lines and Cell Lines

Commercially available cell lines HT29, HCT116, and Colo205 were purchased from the American Type Culture Collection and maintained according to their recommendations. Two additional cell lines HLM482 and HLM566 were generated from fresh material from liver metastases of CRC from two patients. Small pieces of tumor material from a liver metastasis were placed with 1.5 ml of DMEM (containing 10% FCS and 1% penicillin/streptomycin) in a small cell culture flask, cultured at 37°C, and medium was replaced every day. Outgrowing tumor cells were detached using 0.5 ml of Accutase (Merck) and propagated in a new flask.

### Flow Cytometry

For each experiment, tissue from the invasive margin of CRC liver metastases (up to 10 g) was dissociated by cutting and multiple washing steps using a 40-μm cell strainer and RPMI medium. The extracted cells were then placed in a 24-well plate with RPMI medium (supplemented by 10% FCS) overnight and then optionally blocked with Monensin (BD Biosciences) for 3 hr. Cells were then harvested, centrifuged, and analyzed for CD3, CD8, CD4, and CCL5 using flow cytometry standard protocols.

### Invasion Chamber Assays

Standard protocols for invasion chambers were used (Albini and Benelli, 2007). For evaluation of cell invasion, upper chambers of Biocoat Matrigel invasion chambers (8 μm pore size/PET membrane; BD) were seeded with serum-starved

**Figure 5. CCR5 Blockade and Amelioration of the Tumor-Promoting Microenvironment in Human Cancer Patients Leads to Clinical Effects**

(A) MARACON treatment and biomarker assessment schedule. Tumor biopsy sampling and magnetic resonance imaging (MRI) are performed at baseline prior to the first dose of maraviroc and then within the first 4 weeks and 8 weeks for biopsy and MRI, respectively, after the initiation of maraviroc treatment. Patients were monitored for 12 months after completion of the monotherapy treatment phase.

(B) T2-weighted MR image showing the liver (left) and higher magnification of the white rectangular area (right) with arrows indicating other metastases with central necrosis. In right "after" panel, asterisk indicates necrosis and double arrow indicates vital rim. Right "before" panel shows the same metastasis before CCR5 inhibition.

(C) Imaging of lung metastases (indicated by an arrow) before and after 4 weeks of therapy.

(D) Effects of CCR5-inhibition within the biopsy tissue from same lesion before and while under treatment. Tumor areas and corresponding adjacent liver from three patients with hemalaun staining are shown. The patient to the left developed acellular mucinous pools in the tumor, while the two others showed increased necrotic areas, single-cell dissociation, and cell nucleus enlargement of remaining tumor cells. Scale bars, 400 μm.

(E) Cytokine alterations in the invasive margin biopsies in eight patients (nine patients were evaluable for IFN-α2) comparing before treatment and while under treatment.

(F) Representative PET-MRI images from a patient receiving chemotherapy (CHT) after trial participation. White arrow indicates liver with metastatic lesions. Red spots indicate high glucose uptake typical for metastases, and green indicates low background glucose uptake.

(G) Waterfall plot indicating the responses of the chemotherapy treated patients. Single asterisk indicates a patient with a *BRAF* mutant tumor who never had an objective response to any previous therapy. NE** indicates a patient who was not evaluable due to allergic reaction to oxaliplatinum; decrease in serum tumor marker carcinoembryonic antigen was 30% after the second cycle of chemotherapy.

See also Figure S5.

**Table 3. Treatment-Related Adverse Events**

| | Common Toxicity Criteria Grade | | | | |
|---|---|---|---|---|---|
| | 1 | 2 | 3 | 4 | All |
| Alkaline phosphatase | 3 | 2 | 2 | 0 | 6 |
| Alanine aminotransferase increased | 3 | 1 | 1 | 0 | 5 |
| Aspartate aminotransferase increased | 2 | 3 | 1 | 0 | 6 |
| Back pain | 5 | 0 | 0 | 0 | 5 |
| γ-Glutamyltransferase increased | 0 | 0 | 3 | 1 | 4 |
| Blood bilirubin increased | 2 | 1 | 0 | 0 | 3 |
| Hypotension | 3 | 0 | 0 | 0 | 3 |
| Blood lactate dehydrogenase increased | 1 | 1 | 0 | 0 | 2 |
| C-reactive protein increased | 2 | 0 | 0 | 0 | 2 |
| Pyrexia | 1 | 1 | 0 | 0 | 2 |
| Abdominal distension | 1 | 0 | 0 | 0 | 1 |
| Abdominal pain | 2 | 0 | 0 | 0 | 2 |
| Anemia | 1 | 1 | 0 | 0 | 2 |
| Ascites | 1 | 0 | 0 | 0 | 1 |
| Blood creatine phosphokinase MB increased | 1 | 0 | 0 | 0 | 1 |
| Cough | 1 | 0 | 0 | 0 | 1 |
| Device-related infection | 1 | 0 | 0 | 0 | 1 |
| Diarrhea | 1 | 0 | 0 | 0 | 1 |
| Dizziness | 1 | 0 | 0 | 0 | 1 |
| Dysphagia | 1 | 0 | 0 | 0 | 1 |
| Dyspnea | 1 | 0 | 0 | 0 | 1 |
| Endoscopic retrograde cholangiopancreatography | 0 | 1 | 0 | 0 | 1 |
| Fatigue | 0 | 1 | 0 | 0 | 1 |
| Hemorrhage | 1 | 0 | 0 | 0 | 1 |
| Hepatic pain | 1 | 0 | 0 | 0 | 1 |
| Hyperuricemia | 2 | 0 | 0 | 0 | 2 |
| Hypomagnesemia | 1 | 0 | 0 | 0 | 1 |
| Hypothyroidism | 1 | 0 | 0 | 0 | 1 |
| Insomnia | 1 | 0 | 0 | 0 | 1 |
| Leukocytosis | 1 | 0 | 0 | 0 | 1 |
| Myogelosis | 1 | 0 | 0 | 0 | 1 |
| Nasopharyngitis | 0 | 1 | 0 | 0 | 1 |
| Nausea | 1 | 0 | 0 | 0 | 1 |
| Peripheral motor neuropathy | 0 | 1 | 0 | 0 | 1 |
| Platelet count increased | 1 | 0 | 0 | 0 | 1 |
| Pneumonia | 0 | 1 | 0 | 0 | 1 |
| Polyneuropathy | 0 | 1 | 0 | 0 | 1 |
| Procedural pain (biopsy associated) | 1 | 0 | 0 | 0 | 1 |
| Prothrombin time prolonged | 1 | 0 | 0 | 0 | 1 |
| Renal failure, acute | 0 | 1 | 0 | 0 | 1 |
| Sinus congestion | 1 | 0 | 0 | 0 | 1 |
| Skin infection | 1 | 0 | 0 | 0 | 1 |
| Vomiting | 1 | 0 | 0 | 0 | 1 |
| Weight decreased | 1 | 0 | 0 | 0 | 1 |
| All | 51 | 16 | 7 | 1 | 75 |

Grade 1 + 2 events, 89.33%; Grade 3 + 4 events, 10.66%.

(24 hr) tumor cells ($10^5$ cells per 100 μl of medium). The bottom chamber contained MEM with FBS and in half of the wells CCL5 at 10 ng/ml. After 22 hr, non-migrated cells were removed and the membranes with invaded cells were fixed with 33% acetone in methanol and stained with hematoxylin solution, Gill No.3 (1:2 diluted; Sigma-Aldrich). The membranes were then placed on a standard glass slide and mounted with Aquatex (Merck). All cells on the membrane were counted automatically using the VIS software package.

### Western Blotting

Western blotting was performed using standard protocols and according to manufacturer's recommendations (EMT Antibody Sampler Kit; Jak/Stat Pathway Inhibitors Antibody Sampler Kit; STAT3, clone 124H6; New England Biolabs).

### PCR-Based Mutational Profiling

Laser microdissected material was used according to the manufacturer's instructions (Diacarta).

### Horizontal Matrigel Migration Models

Matrigel (undiluted; BD) was evenly plated at the sides of a 24-well chamber in two half-moon shapes (cat's eye configuration) and the remaining third in between was filled with either pure collagen or Matrigel with CXCL9 (10 ng/ml) and CXCL10 (10 ng/ml). After gelling overnight in a humid chamber at 37°C and 5% $CO_2$, the well was filled with a thin layer of T cell culture media and activated T lymphocytes (anti-CD3/anti-CD28 and evaluation by cytokine production), or extracted T cells from tumor tissue were placed on the right half-moon-shaped third. After migration for 48 hr at 37°C, the resulting distribution in the well was documented.

### Organotypic Functional Tumor Explant Models

Resected specimens were used for individual cell culture treatment. In brief, the resected specimen rapidly was transferred to the laboratory in a sterile container, split into equal smaller tissue blocks with each block containing equal proportions of liver metastasis and adjacent liver (size approximately 5 × 3 × 1 mm), and treated. One tissue block was directly frozen in liquid nitrogen, and from another block lysates were generated directly for reference purposes. Further details can be found in Supplemental Experimental Procedures.

### Phase I Clinical Trial

The MARACON-001 phase I trial ("Treatment of Advanced Colorectal Cancer Patients with Hepatic Liver Metastases using the CCR5-Antagonist Maraviroc", clinical trials.gov identifier NCT01736813, EudraCT 2012-000861-18) involves daily exposure to maraviroc (300 mg twice daily), a highly selective CCR5 inhibitor, for 2 months. Safety and feasibility are the primary endpoints of this trial, being conducted according to the Declaration of Helsinki and relevant International Conference on Harmonization Good Clinical Practice guidelines, and with approval from the ethics committee of the University of Heidelberg. All patients had received all current standard-of-care treatment options and were now refractory to standard chemotherapy. For additional details on toxicities and tumor responses (using RECIST criteria for trial participation and follow-up), see Supplemental Experimental Procedures. All patients provided written informed consent before participating in this study.

### Statistical Analyses

Statistical analyses were performed with SPSS 16.0 software. Normality distribution of data was assessed by Wilk-Shapiro tests and, where necessary, QQ plots. For the comparison of different groups, non-parametric exact Mann-Whitney U tests were used. For paired sample analysis the Wilcoxon signed-rank test was used where necessary, and correlation was calculated with Spearman's rank correlation. Multiple comparisons using t tests were corrected with Bonferroni correction. In boxplots the box extends from the 25th to 75th percentiles with the central line being the median, and whiskers stretching from minimum to maximum values. Results with two-tailed p values of $<0.05$ were judged to be statistically significant. All experiments were performed in triplicate unless otherwise noted.

**Table 4. Patients' Treatment Responses Following Maraviroc Treatment**

| Patients | Maraviroc | *BRAF* Mut. | Subsequent Chemotherapy | Objective Response (Comment) |
|---|---|---|---|---|
| Core cohort | | | | |
| 3 | + | neg | FOLFOX4 + bevacizumab | PR |
| 4 | + | pos | FOLFOX4 + bevacizumab | PR (first objective response to a chemotherapy) |
| 9 | + | neg | FOLFIRI (80%) + bevacizumab | PR |
| 10 | + | neg | oxaliplatin + raltitrexed | NE (serum tumor marker decrease 30% after first cycle) |
| 11 | + | neg | FOLFIRI + bevacizumab | SD |
| Extension cohort | | | | |
| 12 | + | neg | capecitabine + bevacizumab | SD |
| 13 | + | neg | capecitabine + bevacizumab | NE (ultrasound evaluation: partial remission) |
| 14 | + | neg | FOLFIRI + bevacizumab | SD |

PR, partial remission; NE, not evaluable; SD, stable disease.
FOLFOX4 is combination chemotherapy consisting of oxaliplatinum, 5-fluorouracil, and folinic acid.
FOLFIRI is combination chemotherapy consisting of irinotecan, 5-fluorouracil, and folinic acid (% dose indicated).

## SUPPLEMENTAL INFORMATION

Supplemental Information includes Supplemental Experimental Procedures, five figures, and one table and can be found with this article online at http://dx.doi.org/10.1016/j.ccell.2016.03.005.

## AUTHOR CONTRIBUTIONS

N.H. conceived the experiments and the study, and N.H. and C.S. designed the study. N.H. coordinated the study with support from J.K. A.B.H., T.L., C.L.M., F.K., N.H., M.S.C., and C.K. performed the laboratory assays and K.B., J.W., M.K., M.S., F.K., A.U., and M.W.B. contributed material. N.H., I.Z., C.F., and L.Z. analyzed and interpreted the data. T.S., N.H., and N.G. provided bioinformatics algorithms. N.H. drafted the article supported by critical revisions from I.Z., D.J., C.F., and L.Z. and important intellectual content provided by F.L., C.K., M.W.B, A.B., J.W., C.B., E.H., N.K., A.U., C.B., T.H., M.K., and J.K. Statistics were performed by A.B., C.K.U., and S.L.

## ACKNOWLEDGMENTS

We thank Ludmila Umansky and Jutta Funk for excellent technical assistance, and Anette Manka-Stuhlik and Nadine Heydrich for trial support. This study was supported by the Dietmar Hopp Foundation, the Helmholtz Alliance 'Immunotherapy of Cancer' (N.H., D.J., C.S.F.), the IFB-Tx, ref. nr. BMBF 01EO1302, and grants of the DFG SFB738 project B8 (C.S.F.) and KFO227 (N.H., M.S., M.K., J.W., M.W.B., D.J., I.Z., C.K., F.K.). Infrastructure at the TIGA center was supported by MEDSYS and GERONTOSYS grants to N.G.

Received: July 17, 2015
Revised: January 27, 2016
Accepted: March 11, 2016
Published: April 11, 2016

## REFERENCES

Abel, S., van der Ryst, E., Rosario, M.C., Ridgway, C.E., Medhurst, C.G., Taylor-Worth, R.J., and Muirhead, G.J. (2008). Assessment of the pharmacokinetics, safety and tolerability of maraviroc, a novel CCR5 antagonist, in healthy volunteers. Br. J. Clin. Pharmacol. *65* (*Suppl 1*), 5–18.

Acharyya, S., Oskarsson, T., Vanharanta, S., Malladi, S., Kim, J., Morris, P.G., Manova-Todorova, K., Leversha, M., Hogg, N., Seshan, V.E., et al. (2012). A CXCL1 paracrine network links cancer chemoresistance and metastasis. Cell *150*, 165–178.

Affara, N.I., Ruffell, B., Medler, T.R., Gunderson, A.J., Johansson, M., Bornstein, S., Bergsland, E., Steinhoff, M., Li, Y., Gong, Q., et al. (2014). B cells regulate macrophage phenotype and response to chemotherapy in squamous carcinomas. Cancer Cell *25*, 809–821.

Albini, A., and Benelli, R. (2007). The chemoinvasion assay: a method to assess tumor and endothelial cell invasion and its modulation. Nat. Protoc. *2*, 504–511.

Arkenau, H.T., Brunetto, A.T., Barriuso, J., Olmos, D., Eaton, D., de Bono, J., Judson, I., and Kaye, S. (2009). Clinical benefit of new targeted agents in phase I trials in patients with advanced colorectal cancer. Oncology *76*, 151–156.

Barashi, N., Weiss, I.D., Wald, O., Wald, H., Beider, K., Abraham, M., Klein, S., Goldenberg, D., Axelrod, J., Pikarsky, E., et al. (2013). Inflammation induced hepatocellular carcinoma is dependent on CCR5. Hepatology *58*, 1021–1030.

Coussens, L.M., Zitvogel, L., and Palucka, A.K. (2013). Neutralizing tumor-promoting chronic inflammation: a magic bullet? Science *339*, 286–291.

DeNardo, D.G., and Coussens, L.M. (2007). Inflammation and breast cancer. Balancing immune response: crosstalk between adaptive and innate immune cells during breast cancer progression. Breast Cancer Res. *9*, 212.

DeNardo, D.G., Brennan, D.J., Rexhepaj, E., Ruffell, B., Shiao, S.L., Madden, S.F., Gallagher, W.M., Wadhwani, N., Keil, S.D., Junaid, S.A., et al. (2011). Leukocyte complexity predicts breast cancer survival and functionally regulates response to chemotherapy. Cancer Discov. *1*, 54–67.

Dorr, P., Westby, M., Dobbs, S., Griffin, P., Irvine, B., Macartney, M., Mori, J., Rickett, G., Smith-Burchnell, C., Napier, C., et al. (2005). Maraviroc (UK-427,857), a potent, orally bioavailable, and selective small-molecule inhibitor of chemokine receptor CCR5 with broad-spectrum anti-human immunodeficiency virus type 1 activity. Antimicrob. Agents Chemother. *49*, 4721–4732.

Dunn, G.P., Old, L.J., and Schreiber, R.D. (2004). The three Es of cancer immunoediting. Annu. Rev. Immunol. *22*, 329–360.

Ellis, L.M., and Fidler, I.J. (2010). Finding the tumor copycat. Therapy fails, patients don't. Nat. Med. *16*, 974–975.

Findeisen, P., Kloor, M., Merx, S., Sutter, C., Woerner, S.M., Dostmann, N., Benner, A., Dondog, B., Pawlita, M., Dippold, W., et al. (2005). T25 repeat in the 3′ untranslated region of the CASP2 gene: a sensitive and specific marker for microsatellite instability in colorectal cancer. Cancer Res. *65*, 8072–8078.

Fridman, W.H., Pages, F., Sautes-Fridman, C., and Galon, J. (2012). The immune contexture in human tumours: impact on clinical outcome. Nat. Rev. Cancer *12*, 298–306.

Gabrilovich, D.I., Ostrand-Rosenberg, S., and Bronte, V. (2012). Coordinated regulation of myeloid cells by tumours. Nat. Rev. Immunol. *12*, 253–268.

Galon, J., Costes, A., Sanchez-Cabo, F., Kirilovsky, A., Mlecnik, B., Lagorce-Pages, C., Tosolini, M., Camus, M., Berger, A., Wind, P., et al. (2006). Type, density, and location of immune cells within human colorectal tumors predict clinical outcome. Science *313*, 1960–1964.

Gonzalez-Martin, A., Mira, E., and Manes, S. (2012). CCR5 in cancer immunotherapy: more than an 'attractive' receptor for T cells. Oncoimmunology *1*, 106–108.

Grothey, A., Van Cutsem, E., Sobrero, A., Siena, S., Falcone, A., Ychou, M., Humblet, Y., Bouche, O., Mineur, L., Barone, C., et al. (2013). Regorafenib monotherapy for previously treated metastatic colorectal cancer (CORRECT): an international, multicentre, randomised, placebo-controlled, phase 3 trial. Lancet *381*, 303–312.

Halama, N., Michel, S., Kloor, M., Zoernig, I., Pommerencke, T., von Knebel Doeberitz, M., Schirmacher, P., Weitz, J., Grabe, N., and Jager, D. (2009a). The localization and density of immune cells in primary tumors of human metastatic colorectal cancer shows an association with response to chemotherapy. Cancer Immun. *9*, 1.

Halama, N., Zoernig, I., Spille, A., Westphal, K., Schirmacher, P., Jaeger, D., and Grabe, N. (2009b). Estimation of immune cell densities in immune cell conglomerates: an approach for high-throughput quantification. PLoS One *4*, e7847.

Halama, N., Zoernig, I., Spille, A., Michel, S., Kloor, M., Grauling-Halama, S., Westphal, K., Schirmacher, P., Jaeger, D., and Grabe, N. (2010). Quantification of prognostic immune cell markers in colorectal cancer using whole slide imaging tumor maps. Anal Quant Cytol. Histol. *32*, 333–340.

Halama, N., Braun, M., Kahlert, C., Spille, A., Quack, C., Rahbari, N., Koch, M., Weitz, J., Kloor, M., Zoernig, I., et al. (2011a). Natural killer cells are scarce in colorectal carcinoma tissue despite high levels of chemokines and cytokines. Clin. Cancer Res. *17*, 678–689.

Halama, N., Michel, S., Kloor, M., Zoernig, I., Benner, A., Spille, A., Pommerencke, T., von Knebel, D.M., Folprecht, G., Luber, B., et al. (2011b). Localization and density of immune cells in the invasive margin of human colorectal cancer liver metastases are prognostic for response to chemotherapy. Cancer Res. *71*, 5670–5677.

Halama, N., Spille, A., Lerchl, T., Brand, K., Herpel, E., Welte, S., Keim, S., Lahrmann, B., Klupp, F., Kahlert, C., et al. (2013). Hepatic metastases of colorectal cancer are rather homogeneous but differ from primary lesions in terms of immune cell infiltration. Oncoimmunology *2*, e24116.

Hales, R.K., Banchereau, J., Ribas, A., Tarhini, A.A., Weber, J.S., Fox, B.A., and Drake, C.G. (2010). Assessing oncologic benefit in clinical trials of immunotherapy agents. Ann. Oncol. *21*, 1944–1951.

Hervas-Stubbs, S., Perez-Gracia, J.L., Rouzaut, A., Sanmamed, M.F., Le Bon, A., and Melero, I. (2011). Direct effects of type I interferons on cells of the immune system. Clin. Cancer Res. *17*, 2619–2627.

Hwang, W.L., Yang, M.H., Tsai, M.L., Lan, H.Y., Su, S.H., Chang, S.C., Teng, H.W., Yang, S.H., Lan, Y.T., Chiou, S.H., et al. (2011). SNAIL regulates interleukin-8 expression, stem cell-like activity, and tumorigenicity of human colorectal carcinoma cells. Gastroenterology *141*, 279–291, 291.e1–5.

Keim, S., Zoernig, I., Spille, A., Lahrmann, B., Brand, K., Herpel, E., Grabe, N., Jager, D., and Halama, N. (2012). Sequential metastases of colorectal cancer: Immunophenotypes and spatial distributions of infiltrating immune cells in relation to time and treatments. Oncoimmunology *1*, 593–599.

Klein, C.A. (2009). Parallel progression of primary tumours and metastases. Nat. Rev. Cancer *9*, 302–312.

Kuang, D.-M., Zhao, Q., Peng, C., Xu, J., Zhang, J.-P., Wu, C., and Zheng, L. (2009). Activated monocytes in peritumoral stroma of hepatocellular carcinoma foster immune privilege and disease progression through PD-L1. J. Exp. Med. *206*, 1327–1337.

Lee, Y., Chittezhath, M., Andre, V., Zhao, H., Poidinger, M., Biondi, A., D'Amico, G., and Biswas, S.K. (2012). Protumoral role of monocytes in human B-cell precursor acute lymphoblastic leukemia: involvement of the chemokine CXCL10. Blood *119*, 227–237.

Liou, G.Y., Doppler, H., Necela, B., Krishna, M., Crawford, H.C., Raimondo, M., and Storz, P. (2013). Macrophage-secreted cytokines drive pancreatic acinar-to-ductal metaplasia through NF-kappaB and MMPs. J. Cell Biol. *202*, 563–577.

Melero, I., Hervas-Stubbs, S., Glennie, M., Pardoll, D.M., and Chen, L. (2007). Immunostimulatory monoclonal antibodies for cancer therapy. Nat. Rev. Cancer *7*, 95–106.

Mlecnik, B., Tosolini, M., Charoentong, P., Kirilovsky, A., Bindea, G., Berger, A., Camus, M., Gillard, M., Bruneval, P., Fridman, W.H., et al. (2009). Biomolecular network reconstruction identifies T cell homing factors associated with survival in colorectal cancer. Gastroenterology *138*, 1429–1440.

Musha, H., Ohtani, H., Mizoi, T., Kinouchi, M., Nakayama, T., Shiiba, K., Miyagawa, K., Nagura, H., Yoshie, O., and Sasaki, I. (2005). Selective infiltration of CCR5(+)CXCR3(+) T lymphocytes in human colorectal carcinoma. Int. J. Cancer *116*, 949–956.

Nielsen, D.L., Palshof, J.A., Larsen, F.O., Jensen, B.V., and Pfeiffer, P. (2014). A systematic review of salvage therapy to patients with metastatic colorectal cancer previously treated with fluorouracil, oxaliplatin and irinotecan +/− targeted therapy. Cancer Treat Rev. *40*, 701–715.

Oppermann, M. (2004). Chemokine receptor CCR5: insights into structure, function, and regulation. Cell Signal. *16*, 1201–1210.

Pardoll, D.M. (2012). The blockade of immune checkpoints in cancer immunotherapy. Nat. Rev. Cancer *12*, 252–264.

Qian, B.Z., and Pollard, J.W. (2012). New tricks for metastasis-associated macrophages. Breast Cancer Res. *14*, 316.

Qin, H., Holdbrooks, A.T., Liu, Y., Reynolds, S.L., Yanagisawa, L.L., and Benveniste, E.N. (2012). SOCS3 deficiency promotes M1 macrophage polarization and inflammation. J. Immunol. *189*, 3439–3448.

Reshef, R., Luger, S.M., Hexner, E.O., Loren, A.W., Frey, N.V., Nasta, S.D., Goldstein, S.C., Stadtmauer, E.A., Smith, J., Bailey, S., et al. (2012). Blockade of lymphocyte chemotaxis in visceral graft-versus-host disease. N. Engl. J. Med. *367*, 135–145.

Sethi, N., and Kang, Y. (2011). Unravelling the complexity of metastasis—molecular understanding and targeted therapies. Nat. Rev. Cancer *11*, 735–748.

Sistigu, A., Yamazaki, T., Vacchelli, E., Chaba, K., Enot, D.P., Adam, J., Vitale, I., Goubar, A., Baracco, E.E., Remedios, C., et al. (2014). Cancer cell-autonomous contribution of type I interferon signaling to the efficacy of chemotherapy. Nat. Med. *20*, 1301–1309.

Stewart, T.J., and Smyth, M.J. (2009). Chemokine-chemokine receptors in cancer immunotherapy. Immunotherapy *1*, 109–127.

Topalian, S.L., Drake, C.G., and Pardoll, D.M. (2012). Targeting the PD-1/B7-H1(PD-L1) pathway to activate anti-tumor immunity. Curr. Opin. Immunol. *24*, 207–212.

Trinchieri, G. (2010). Type I interferon: friend or foe? J. Exp. Med. *207*, 2053–2063.

Van Cutsem, E., Kohne, C.-H., Hitre, E., Zaluski, J., Chang Chien, C.-R., Makhson, A., D'Haens, G., Pinter, T., Lim, R., Bodoky, G., et al. (2009). Cetuximab and chemotherapy as initial treatment for metastatic colorectal cancer. N. Engl. J. Med. *360*, 1408–1417.

Vanneman, M., and Dranoff, G. (2012). Combining immunotherapy and targeted therapies in cancer treatment. Nat. Rev. Cancer *12*, 237–251.

Velasco-Velazquez, M., Jiao, X., De La Fuente, M., Pestell, T.G., Ertel, A., Lisanti, M.P., and Pestell, R.G. (2012). CCR5 antagonist blocks metastasis of basal breast cancer cells. Cancer Res. *72*, 3839–3850.

Yan, X., Orentas, R.J., and Johnson, B.D. (2006). Tumor-derived macrophage migration inhibitory factor (MIF) inhibits T lymphocyte activation. Cytokine *33*, 188–198.

Zhou, Q., Yan, X., Gershan, J., Orentas, R.J., and Johnson, B.D. (2008). Expression of macrophage migration inhibitory factor by neuroblastoma leads to the inhibition of antitumor T cell reactivity in vivo. J. Immunol. *181*, 1877–1886.

Zitvogel, L., Apetoh, L., Ghiringhelli, F., Andre, F., Tesniere, A., and Kroemer, G. (2008). The anticancer immune response: indispensable for therapeutic success? J. Clin. Invest. *118*, 1991–2001.

**Cancer Cell, Volume *29***

## Supplemental Information

# Tumoral Immune Cell Exploitation in Colorectal Cancer Metastases Can Be Targeted Effectively by Anti-CCR5 Therapy in Cancer Patients

**Niels Halama, Inka Zoernig, Anna Berthel, Christoph Kahlert, Fee Klupp, Meggy Suarez-Carmona, Thomas Suetterlin, Karsten Brand, Juergen Krauss, Felix Lasitschka, Tina Lerchl, Claudia Luckner-Minden, Alexis Ulrich, Moritz Koch, Juergen Weitz, Martin Schneider, Markus W. Buechler, Laurence Zitvogel, Thomas Herrmann, Axel Benner, Christina Kunz, Stephan Luecke, Christoph Springfeld, Niels Grabe, Christine S. Falk, and Dirk Jaeger**

# Supplemental Data

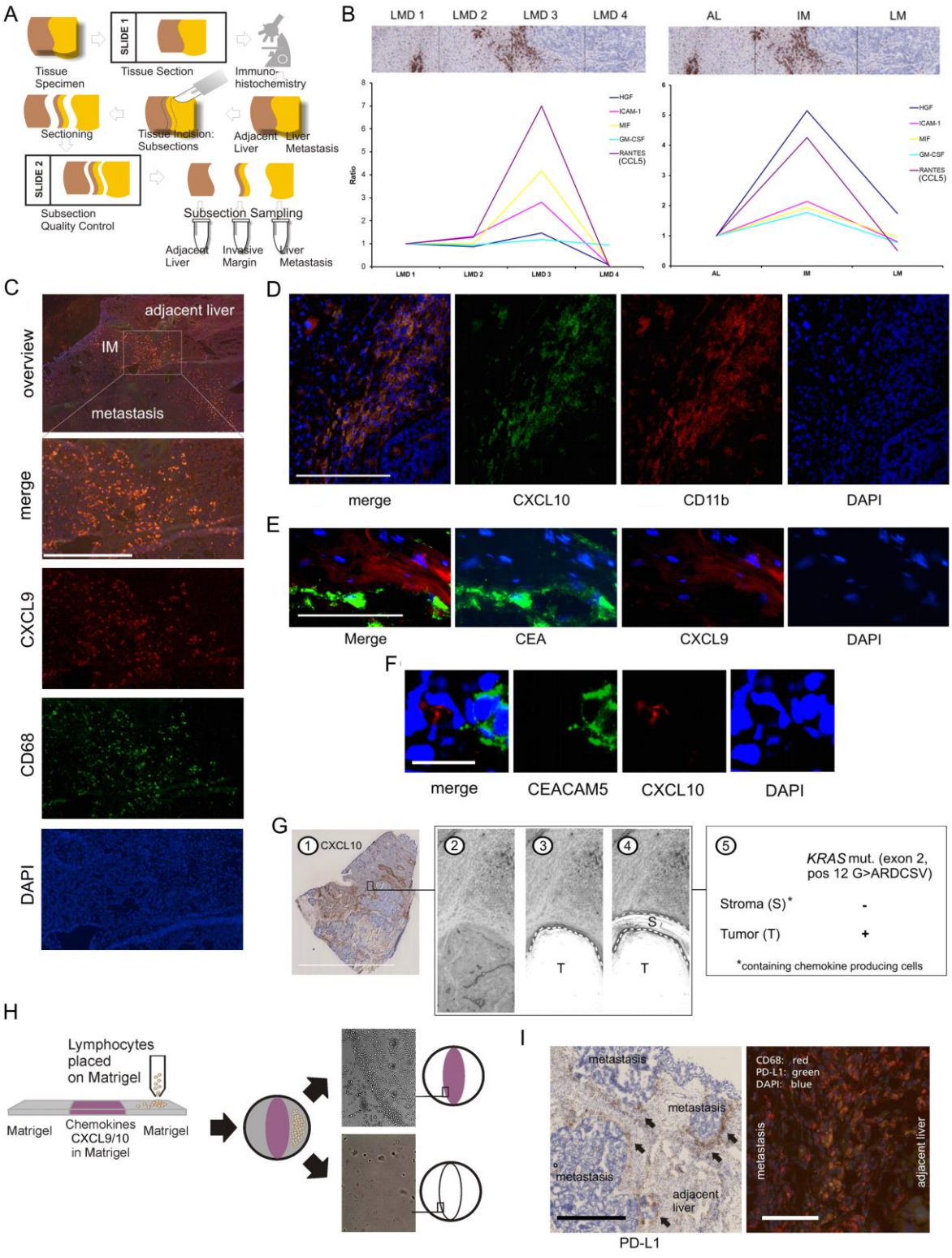


**Figure S1. Related to Figure 1**

(A) Schematic representation of the procedure for subsection acquisition.

(B) Side by side comparison of larger macrodissected specimen ratios to laser-assisted microdissected smaller regions. Upper: laser microdissection was used to dissect four 100 x 100 µm regions across the invasive margin into adjacent liver (left) and liver metastasis (right), adjacent liver was used for the calculation of the ratio as reference. Lower: macrodissected specimen of approximately 500 µm in each direction for the different regions.
(C) Immunofluorescent double staining for CXCL9 (red) and CD68 (green) at the invasive margin. Scale bars 600 µm.
(D) Immunofluorescent double staining for CXCL10 (green) and CD11b (red) at the invasive margin. Scale bar 200 µm.
(E) Immunofluorescent double staining for CXCL9 (red) and CEAMCAM5 (green) (scale bar 100 µm).
(F) Immunofluorescent double staining for CXCL10 (red) and CEAMCAM5 (green) (scale bar 25 µm).
(G) Mutational profiling (using PCR based qClamp mutation specific amplification) of CXCL9/CXCL10 producing cells at the invasive margin (stroma). Scale bar 10 mm.
(H) Horizontal migration experiments with lymphocytes placed on either the chemokine-containing matrigel (left, purple marked matrigel) or on chemokine-free matrigel (right, clear marked matrigel). Petri dish images show representative lymphocyte densities at the specified position.
(I) Spatial distribution of PD-L1 at the metastatic site. Left: Staining for PD-L1 expression, black arrows indicate regions with strong PD-L1 expression, scale bar 800 µm. Right: Immunofluoresecent triple staining, showing CD68 and PD-L1 positive cells at the invasive margin. Scale bar 200 µm.

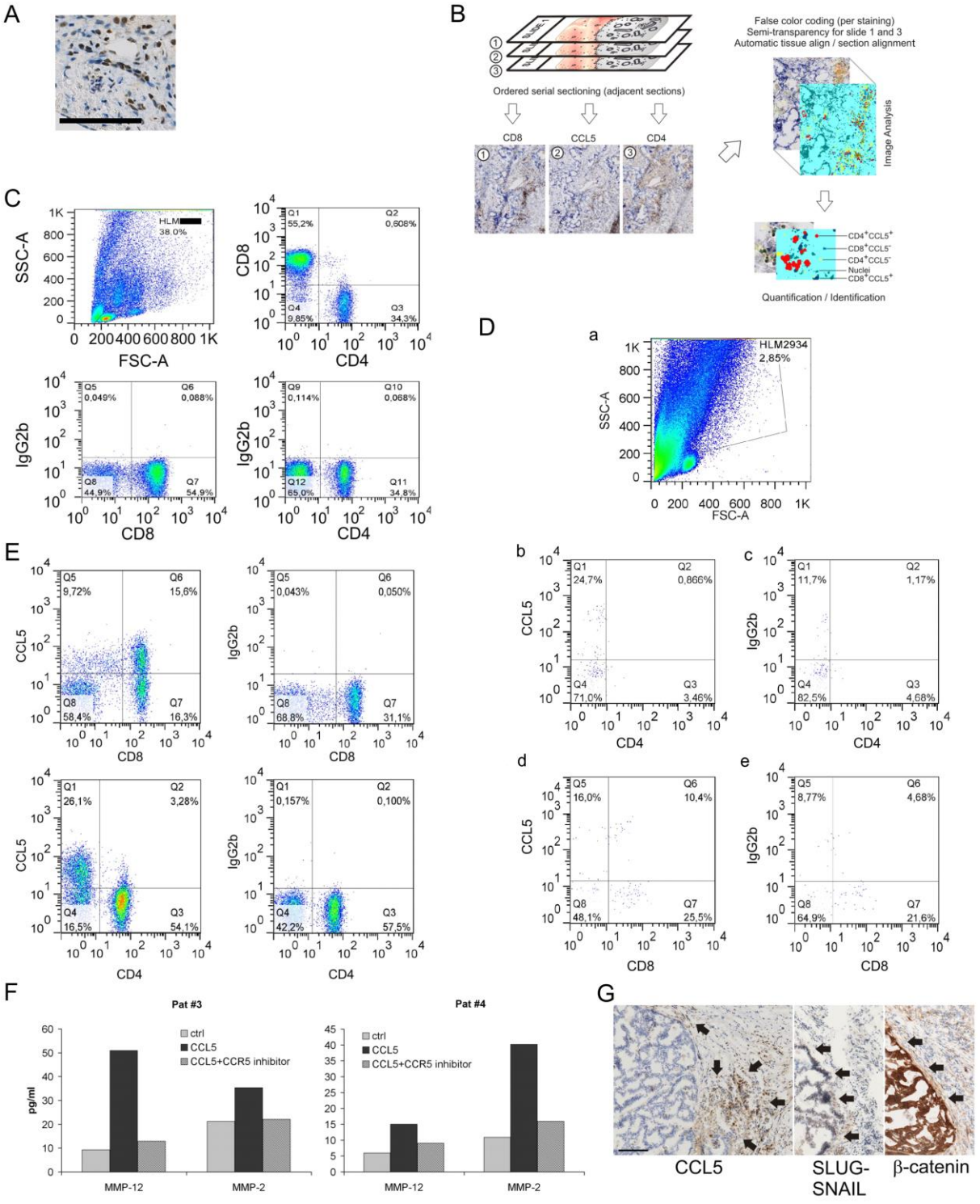
A
B
False color coding (per staining)
Semi-transparency for slide 1 and 3
Automatic tissue align / section alignment
Ordered serial sectioning (adjacent sections)
CD8
CCL5
CD4
Image Analysis
CD4+CCL5+
CD8+CCL5-
CD4+CCL5-
Nuclei
CD8+CCL5+
Quantification / Identification
C
SSC-A
FSC-A
HLM
38.0%
CD8
CD4
IgG2b
D
a
HLM2934
2,85%
b
c
d
e
E
CCL5
IgG2b
F
Pat #3
Pat #4
ctrl
CCL5
CCL5+CCR5 inhibitor
pg/ml
MMP-12
MMP-2
G
CCL5
SLUG-
SNAIL
β-catenin
H
CCL5
CCR5 inhib.
Vimentin
p38
β-tubulin
SNAIL
E-cadherin
β-tubulin

**Figure S2. Related to Figure 2**

**(**A**)** Periportal liver area showing CCR5 positive lymphocytes and macrophages. Scale bar 200 µm.

(B) Virtual triple stain (overlay, schematic view). Attributed pixels are enlarged for better visibility within the image.

(C) FACS analysis of the invasive margin of a colorectal cancer liver metastasis. Forward/sideward scatter plot (upper left panel), $CD4^+$ and $CD8^+$ populations gated on $CD3^+$ (upper right) and isotype controls for CCL5 (CD8 shown in lower left and CD4 in lower right).

**(**D**)** FACS analysis of the invasive margin of a colorectal cancer liver metastasis. Gating on the region of $CD3^-$ cells (a) yields no significant $CCL5^+$ cell numbers in the $CD3^-$ population (CD4 in (b) and CD8 in (c) with isotype control shown in (d) and (e) respectively).

**(**E**)** FACS analysis of donor peripheral blood cells as positive control (left plots CD8 and CD4 and CCL5, right plots CD8 and CD4 and isotype control).

**(**F**)** Matrix-Metalloproteinase levels produced by tumor-associated macrophages upon stimulation with CCL5 (5 ng/ml) or CCL5 and CCR5 inhibitor (4 nM).

**(**G**)** Spatial registry of CCL5 (left), SLUG-SNAIL (middle) and β-catenin (right) within the invasive margin of liver metastases (representative image). While CCL5 shows localization within the peritumoral stroma close to the tumor cells (black arrows), SLUG-SNAIL and β-catenin as components of EMT are typically found at the invasive margin of metastases. Scale bar 400 µm.

**(**H**)** Western blot results for key epithelial-to-mesenchymal transition (EMT) proteins from explant culture of a colorectal cancer liver metastasis tissue sample (with CCL5 5 ng/ml or CCR5 inhibitor (4 nM), three western blots with either p38 or β-tubulin as reference).

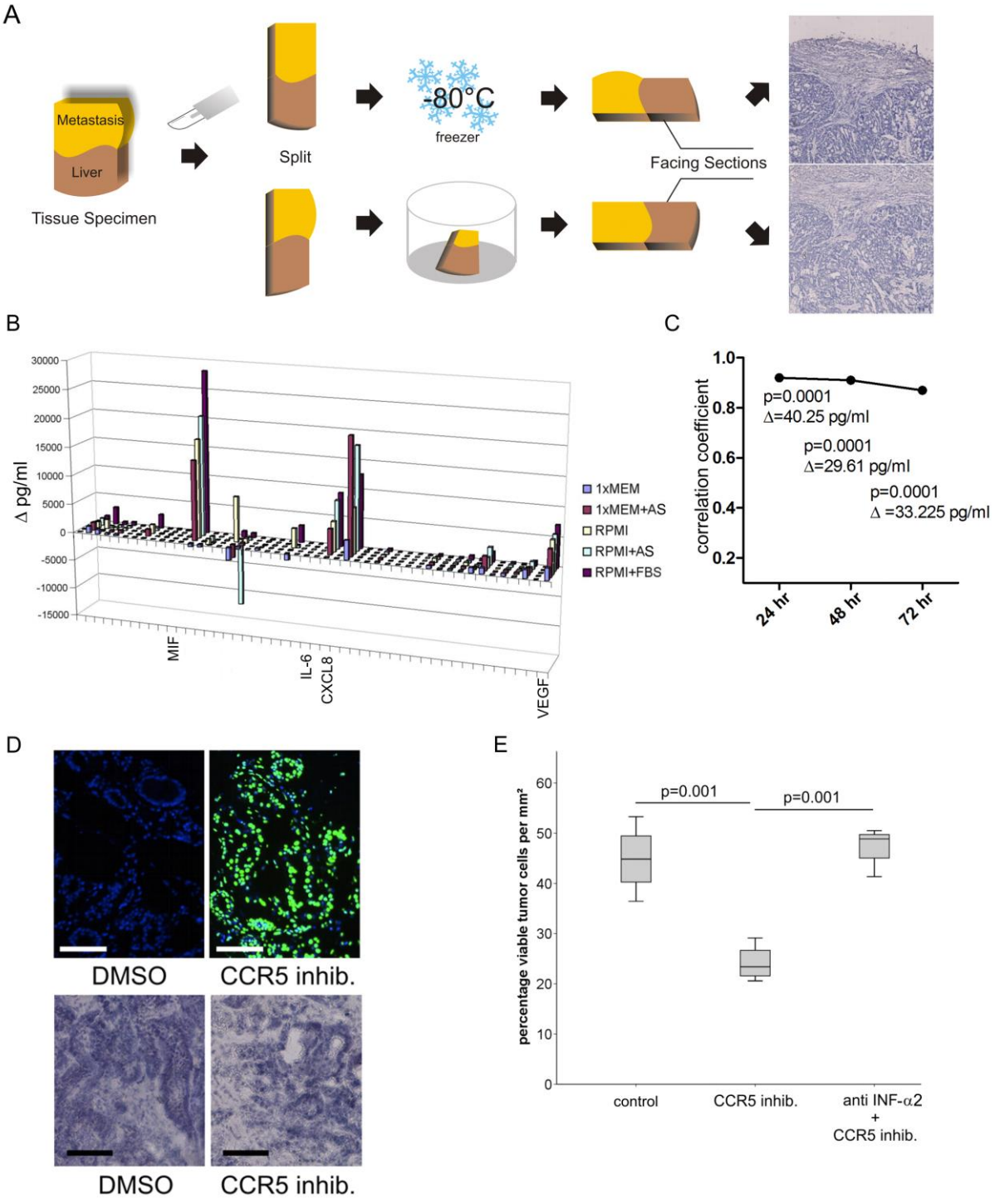


**Figure S3. Related to Figure 3.**

(A) Assessment of morphological changes over time of explant tissue in culture. Directly frozen material is sectioned (upper section) and directly compared to the section of the facing corresponding material after 48 hr of culture (MEM medium) on the lower section (hemalaun stainings).

(B) Comparison of the effects of the medium on the patterns of cytokine and chemokine alterations as compared to the directly frozen reference tissue part (48 hr). Y-axis shows the difference to the reference measurements with absolute values (pg/ml). Grossly altered cytokines are displayed. MEM=Minimum Essential Medium, RPMI=RPMI-1640, FBS=fetal bovine serum, AS=ascites supernatant.

(C) Comparison of different time points, comparing the reference tissue measurements of 50 cytokines to the given time point using MEM medium as outlined above. Statistics given indicate for each pair of measurements the Spearman's rank correlation coefficient rho (y-axis) and the corresponding p values as well as the median absolute differences between the analyzed tissues (reference tissue vs. untreated explant). Time series with patient material (adjacent liver, AL) over 72 hr. A fresh tissue sample was cut into five equally sized pieces, one piece being directly frozen whereas the other four were treated as outlined above and harvested at the given time points. This experiment revealed significant stability of the cytokine patterns within the explant model system over the first 36 to 48 hr.

(D) Example TUNEL staining on explant model sections (+/- CCR5 inhibition) as well as representative counterstained sections (scale bar 100 µm). Comparison between TUNEL staining versus morphological analysis showed an excellent correlation as reported previously and therefore the morphological analysis was used to evaluate effects also in patient biopsies (Duan et al., 2003), H&E staining not shown.

(E) Effects of blocking IFN-α2 with a blocking antibody (10 µg/ml) combined with CCR5 inhibitor (4 nM) on the percentage of viable tumor cells per $mm^2$ (n=5 per group, 48 hr) compared to CCR5 inhibition alone.

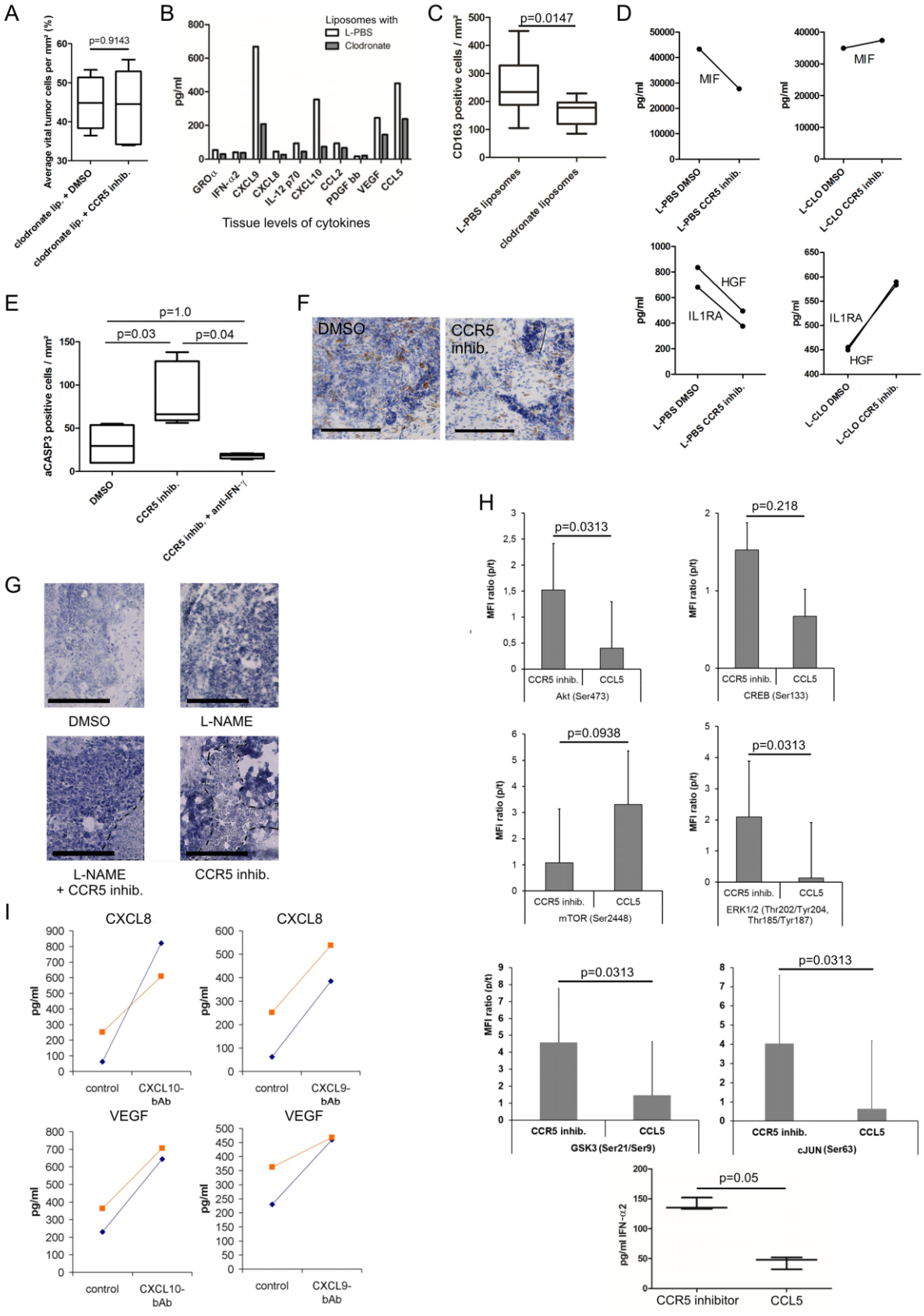
A
Average vital tumor cells per mm² (%)
p=0.9143
clodronate lip. + DMSO
clodronate lip. + CCR5 inhib.
B
Liposomes with
L-PBS
Clodronate
pg/ml
GROα
IFN-α2
CXCL9
CXCL8
IL-12 p70
CXCL10
CCL2
PDGF bb
VEGF
CCL5
Tissue levels of cytokines
C
CD163 positive cells / mm²
p=0.0147
L-PBS liposomes
clodronate liposomes
D
pg/ml
MIF
L-PBS DMSO
L-PBS CCR5 inhib.
L-CLO DMSO
L-CLO CCR5 inhib.
HGF
IL1RA
E
aCASP3 positive cells / mm²
p=1.0
p=0.03
p=0.04
DMSO
CCR5 inhib.
CCR5 inhib. + anti-IFN-γ
F
DMSO
CCR5 inhib.
G
DMSO
L-NAME
L-NAME + CCR5 inhib.
CCR5 inhib.
H
MFI ratio (p/t)
p=0.0313
CCR5 inhib.
CCL5
Akt (Ser473)
p=0.218
CREB (Ser133)
p=0.0938
mTOR (Ser2448)
p=0.0313
ERK1/2 (Thr202/Tyr204, Thr185/Tyr187)
p=0.0313
GSK3 (Ser21/Ser9)
p=0.0313
cJUN (Ser63)
p=0.05
pg/ml IFN-α2
CCR5 inhibitor
CCL5
I
CXCL8
pg/ml
control
CXCL10-bAb
CXCL9-bAb
VEGF

**Figure S4. Related to Figure 4.**

(A) Effects of liposomal clodronate on vital tumor cell content of tissue (explant model, n=5 per group, difference not statistically significant, boxplots shown).

(B) Tissue levels of cytokines in a tumor tissue explant without (white bars, LPS liposomes, 1:10) or with (grey bars, clodronate liposomes) clodronate (1:10, treatment for 48 hr).

(C) $CD163^+$ cell quantities on sections of PBS liposome treated or clodronate liposome treated tumor tissue explants (boxplots, n=5).

(D) Effects of liposomal clodronate (1:10) or liposomal PBS (1:10) with CCR5 inhibitor (or DMSO) on key cytokine levels within the explant model (treatment 48 hr).

(E) Numbers of stromal activated Caspase 3 positive cells under treatment with a CCR5 inhibitor (4 nM) are increased. Interferon gamma inhibiting antibody (2.5 µg/ml) abrogates this increase. Corresponding tissue sections were stained for activated Caspase 3 and positive cells within the stroma were quantified (n=5 explants). Virtual double stain showed double positive $CD163^+CASP3^+$ macrophages (data not shown).

(F) Representative CD163 stainings with/without CCR5 inhibitor. Scale bar 200 µm.

(G) Inhibition of reactive oxygen species production through L-NAME partially blocks tumor cell depletion of CCR5 inhibition (4 nM). Dashed lines indicate areas of overt tumor cell death (scale bar 200 µm). Concentrations of L-NAME (0.1 mM) were used as reported previously.

(H) Changes in phosphoprotein levels (phosphoprotein to total protein levels, as described previously by (Conzelmann et al., 2010)) in tumor-associated macrophages (CCL5 2500 pg/ml) with or without CCR5 inhibition (errorbars indicate s.e.m., n=6, Wilcoxon signed rank test). Corresponding interferon alpha 2 levels are shown below phosphoproteins as boxplots (n=3).

(I) Observed cytokine alterations induced by selective blockade of either CXCL9 or CXCL10 (through blocking antibodies indicated by "bAb", two explant models from two patients), control indicates the untreated reference tissue specimen.

**Table S1, related to Table 1**

| Patients | Localization | Time from first metastasis to trial in months | Comments |
|---|---|---|---|
| Core cohort | | | |
| 1 | Colon | 31.5 | regorafenib (2 months plus two months BSC) |
| 2 | Colon | 16.27 | |
| 3 | Colon | 12.2 | |
| 4 | Colon | 7.13 | |
| 5 | Rectum | 34.57 | |
| 6 | Colon | 62.97 | |
| 7 | Colon | 28.37 | |
| 8 | Rectum | 32.47 | regorafenib (2 months) |
| 9 | Rectum | 91.3 | |
| 10 | Colon | 11.13 | |
| 11 | Colon | 89.33 | |
| Extension cohort | | | |
| 12 | Colon | 70 | regorafenib (3 months) |
| 13 | Rectum | 18.37 | regorafenib (4 months), ascites |
| 14 | Colon | 25,4 | |

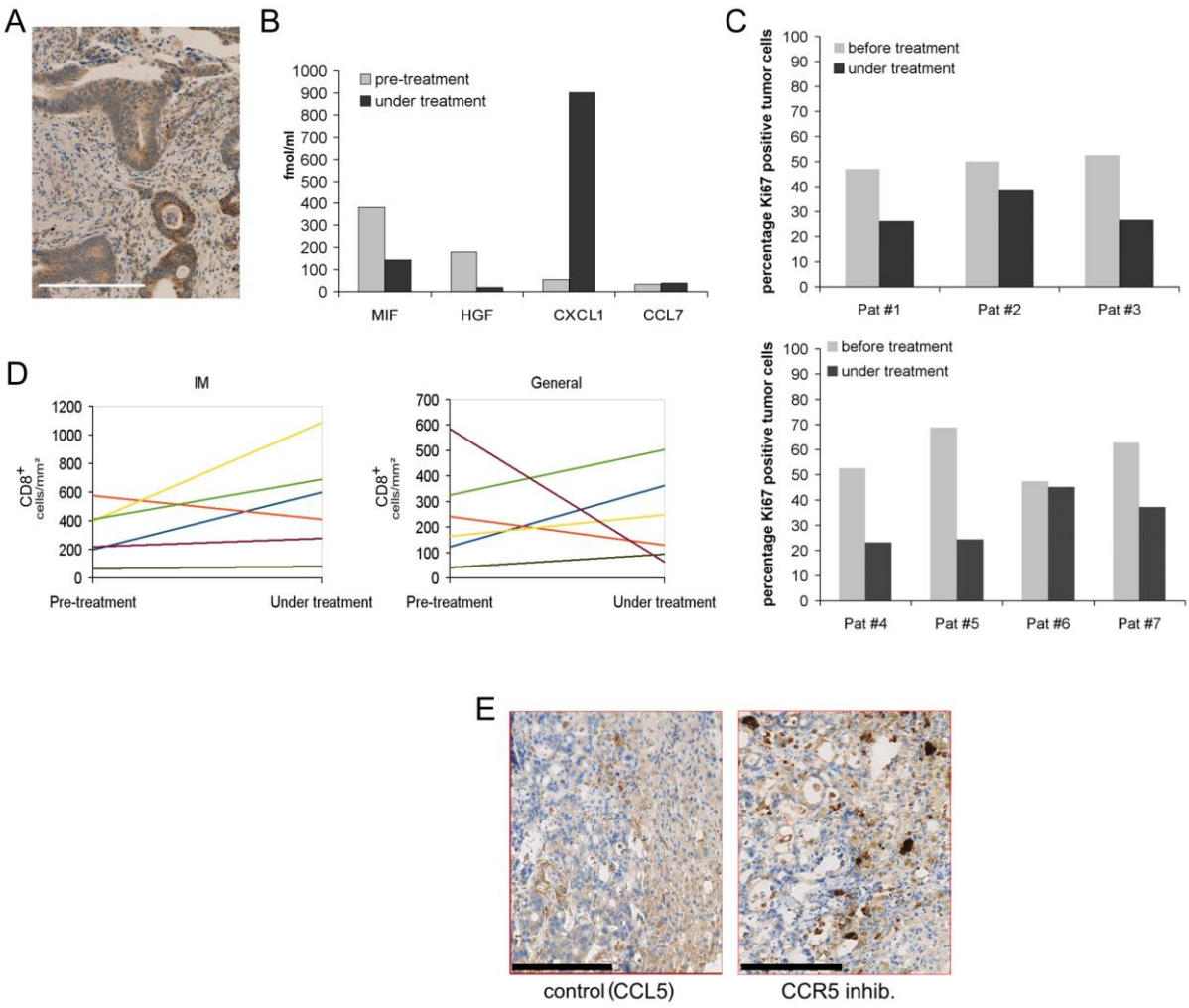


**Figure S5. Related to Figure 5.**

(A) CCR5 staining of a lung metastasis (before treatment with maraviroc) that recurred shortly after resection and progressed under an oxaliplatinum-based therapy (scale bar 200 µm). Note also ample CCR5 expression by stroma-resident cells.

(B) Specific pattern of cytokine alterations in a pleural effusion of one of the patients treated with maraviroc.

(C) Percentages of (remaining) Ki67 positive tumor cells before and under treatment (8-10 days, second biopsy) from the patients as shown in Figure 5.

(D) CD8 cell densities measured with whole slide immune cell quantification within the invasive margin (IM, left) and the remaining other tissue (general, right). In 5 of 6 cases the CD8 density increased or remained stable under treatment at the invasive margin.

(E) Representative example of changes in density of IFN-α2-positive cells before and under CCR5 inhibition in a patient from the MARACON trial (staining with anti-IFN-α2 antibody, DAB, scale bar 200 µm).

# Supplemental Experimental Procedures

## Cell culture & Proliferation assays.

T cells were drawn from healthy donors and after a short period of rest were stimulated in CD3/CD28 coated 96 well plates (anti-CD3 from BioLegend, USA, anti-CD8 from BD, Germany) overnight. T cell culture media contained RPMI 1640 (PAA, USA), 10% human serum (heat-inactivated for 30 minutes at 56 °C), 1% Glutamine (PAA, USA), 1% penicillin/streptomycine (PAA, USA), 1% Non-essential amino acids (PAA, USA) and 1% HEPES (PAA, USA). Commercial tumor cell lines were cultured according to the suppliers instructions. Quantification of cells was performed in triplicates with double measurements with the automated cell counter TC10 (BioRad, Germany), especially directly after seeding (i.e. $0.5 * 10^5$ cells /ml for proliferation assays, cells equally seeded in plates) and after incubation/treatment. Primary cell lines were authenticated using Multiplex Cell Authentication by Multiplexion (Heidelberg, Germany) as described recently (Castro et al., 2013). The SNP profiles matched known profiles were unique, consistent with a human epithelial tumor cell line. All cell lines were tested for Mycoplasma contamination by PCR.

Preparation of ascites (from colorectal cancer patients) and extraction of macrophages and lymphocytes was performed as follows. Adapted from previous reports ascites was collected into sterile plastic bags. The outlet nozzle of each bag was prepared by desinfection with 70% alcohol and the first fraction of ascites is discarded while the remaining ascites is distributed in 50 ml Falcon tubes. Centrifugation with 1500 rpm for 10 min. Supernatants were mixed with RPMI medium (1:2) and used as conditioned medium (CM). For macrophage populations (a), pellets were then resuspended in RPMI medium and are run through a Ficoll gradient (30 min at 2000 rpm at room temperature). The interphase was then collected in RPMI, washed and centrifuged (1800 rpm for 10 min) and the resulting pellets are are then seeded into cell flasks with RPMI. For macrophage populations the supernatants were then harvested after an adherence step of 1,5h (37°C), the remaining adherent cells were washed with PBS (three times) and then supplemented with CM. For lymphocytes (b), pellets were then resuspended in RPMI medium centrifuged again and pellets were then seeded into cell flasks with RPMI. After adherence, the supernatant was used to extract lymphocytes. After experiments with either the macrophages or lymphocytes the supernatant was measured for cytokines and the cells were harvested and analyzed with stainings (double staining CD163 and CD68 for macrophages, CEA for tumor cells and CD3 for lymphocytes) and controlled for purity of cell content (>95%). Extraction of tumor cells was performed after dissociation of tumor tissue and adhesion steps as published previously.

## Cytokine & Chemokine Quantification.

A two-laser array reader simultaneously quantifies all cytokines and chemokines of interest. Standard curves and concentrations were calculated with Bio-Plex Manager 4.1.1 on the basis of the 5-parameter logistic plot regression formula. Briefly, small pieces of dissected frozen tissue were transferred in 150 µl cold lysis buffer, vortexed, frozen at – 80°C (10 min) and thawed on ice. After incubation in a cold ultrasonic bath (10 min), samples were frozen again at -80°C, thawed on ice and centrifuged (13.000 rpm, 20 min, 4°C). The protein concentration of the supernatant was determined and the concentration of lysates was adjusted to 1000 µg/ml (300 µg/ml for biopsies) using human serum diluent (BioRad) and cytokine/chemokine concentrations in tissue

lysates were quantified by multiplex protein arrays, according to manufacturer's instructions (BioRad Laboratories, Hercules, CA, USA). The detection sensitivity of the analytes ranged from 1 pg / ml to 100 ng / ml. Values that were identified as "Out of range" by the platform were extrapolated based on the single standard curves that were generated for each analyte. As standard curves showed minimal standard deviations the highest concentrated standard concentration was used for the extrapolation. To form classes of cytokines (in descending order e.g. TH1, TH2, TH17 etc.) the AMIGO database was used (http://amigo.geneontology.org/) in evaluating specific terms (e.g. GO:0043030: regulation of macrophage activation, GO:0042104: positive regulation of activated T cell proliferation or GO:0006935: chemotaxis) or literature search. Positive controls from samples with TH1, TH2 or TH17 dominated cytokines were used for analysis.
General reproducibility (precision) of the multiplex protein quantification approach on serial sections showed an excellent reproducibility (Spearman's Rank correlation with r=0.975 and p=0.0001, median difference 70 pg/ml). Accuracy was evaluated in measurements of solutions with known concentrations of the cytokine, e.g. CCL5 at 25.000 pg/ml which showed a standard deviation of 628.92 pg/ml, corresponding to 2.5% from the expected value and CCL5 at 100 pg/ml which showed a standard deviation of 2.7 pg/ml, corresponding to 2.7% from the expected value. Calibration of the investigated analytes is performed as recommended by the manufacturer (BioRad, Germany) and we refer to the manufacturer's homepage for additional reference material on accuracy and precision (http://www.bio-rad.com/webroot/web/pdf/lsr/literature/Bulletin_5803A.pdf). The general approach for generating subsections is outlined in **Figure S1A**.

Comparison between different serial section invasive margin protein quantifications also revealed an excellent reproducibility (spearman's rank correlation rho=0.922, p=0.0001). Finally the comparison of the ratios of laser-assisted microdissected material to macrodissected material revealed that the invasive margin indeed is a precisely separated region with reproducible and distinct cytokine profiles (see **Figure S1B**). Also, the differences to the surrounding adjacent liver or the liver metastasis are so pronounced that the macrodissected specimen completely resembles the patterns found in the microdissected specimen.

Generation of cytokine and chemokine data from biopsy material of the MARACON-001 was performed as outlined above. Due to the limitations in the amount of material available, the protein concentrations used for the assays was set to 300 mg. Histologically the adjacent liver of the patients remained unchanged under treatment as compared to before treatment, with respect to morphology and immune cell presence. Therefore, as control for the precision of the cytokine measurement (and to assess effects of dilution etc.) the cytokine levels of the adjacent liver before and under treatment were used and showed excellent concordance (spearman's rank correlation rho=0.991 and p=0.0001, median difference 5 pg/ml). This also makes effects of wound healing (that should not be present anymore after day 8 post-biopsy) unlikely to interfere with the effects of CCR5 inhibition. The percentage of apoptotic tumor cells was determined by counting apoptotic nuclei (based on nuclear morphology) and intact tumor cells in sections stained with hemalaun and/or H&E as described previously (Duan et al., 2003).

## Immunohistochemistry & Immunofluorescence.

FFPE tissues were deparaffinized and rehydrated (BOND Dewax Solution, Leica, Germany). After heat-induced epitope retrieval (HIER) at 100 °C (BOND Epitope Retrieval Solution 1 or 2, Leica, Germany), endogenous

peroxidase activity was blocked by incubation with 3% peroxide block for 20 min (BOND Polymer Refine Detection System, Leica, Germany). The sections were blocked with 10% normal goat serum (Vector, USA). A list of the used antibodies and dilutions can be found below. These were applied as primary antibodies at room temperature for 30 min. The slides were incubated with a secondary antibody (rabbit-anti-mouse IgG, Bond Polymer Refine Detection System, Leica, Germany) for 8 min at room temperature. Further amplification of the signal was achieved through incubation with a third antibody, conjugated with horse radish peroxidase and coupled to dextrane molecules in large numbers, for 8 min at room temperature (Poly-HRP-mouse-anti-rabbit IgG, Bond Polymer Refine Detection System, Leica, Germany). The antigen detection was performed by a color reaction with 3,3-di-amino-benzidine (DAB chromogen, Bond Polymer Refine Detection System, Leica, Germany). The sections were counterstained with hematoxylin (Bond Polymer Refine Detection System, Leica, Germany) and mounted with Aquatex (Merck, Germany). Matched isotype controls were used a negative control and adjacent normal tissue or known positive cells were used as positive control.

Immunofluorescence double staining was performed on cryosections using a red fluorescence Alexa Fluor 594 dye-labeled donkey-anti-mouse IgG (Life Technologies, Germany) and a green fluorescence Alexa 488 dye-labeled goat-anti-rabbit IgG (Life Technologies, Germany) sequentially for the chemokine double stainings (or in case of green fluorescence Alexa 488 dye-labeled goat-anti-mouse IgG the second primary antibody was omitted for control). For the analysis of CD68, PD-L1, CD4, CD8 and CCL5 a red fluorescence Alexa Fluor 594 dye-labeled donkey anti-rabbit IgG (Invitrogen, Germany) and a green fluorescence Alexa 488 dye-labeled goat-anti-mouse IgG (Life Technologies, Germany) were used simultaneously. For the analysis of CD3 and CCL5 Alexa Fluor555 goat anti-mouse IgG (H+L) molecular probes A21422 and Alexa Fluor 488 goat anti-rabbit IgG were used. Cryo sections were fixed either with 4% PFA or 33% acetone in methanol prior to staining according to antibody recommendations. After incubation of the first primary antibody overnight at 4 °C, Alexa Fluor 594 (1:100 dilution) was applied for 1 hour. The second primary antibody was applied for 3 hours at room temperature and detected with Alexa Fluor 488 (1:100 dilution) for 1 hour during sequential double staining. For simultaneous staining both primary antibodies were incubated overnight following both Alexa Fluor antibodies (1:100 dilution each) for 1 hour. Sections were mounted using Vectashield with DAPI (Vector, USA) for counterstain. Confocal images were obtained on a Nikon C2 Plus confocal microscope system.

Mouse monoclonal antibodies recognizing human CD3epsilon (1:100 dilution and HIER1 for FFPE, 4% PFA fixation and HIER2 for cryo sections, clone PS1, Novocastra, UK and rabbit monoclonal anti-CD3, clone Sp7 from Abcam), CD8 (1:50 dilution and HIER2 for FFPE, 1:100 dilution and 4% PFA fixation and for cryo sections, clone 4B11, Novocastra, UK), CCR5 (1:50 dilution and HIER1 for FFPE, 1:100 dilution, 4% PFA fixation and HIER1 for cryo sections, clone MM0065-6H20, abcam, UK), CCL5 (1:50 dilution and 4% PFA fixation for cryo sections, clone VL1, BioLegend, USA), PD1 (1:50 dilution and HIER1 for FFPE, 33% acetone in methanol fixation for cryo sections, clone NAT, abcam, UK), CD68 (1:200 dilution and HIER1 for FFPE, 1:700 dilution and 33% acetone in methanol fixation for cryo sections, clone KP1, abcam, UK), CD163 (1:500 dilution and HIER2 for FFPE, 33% acetone in methanol fixation for cryo sections, clone EDHu-1, AbD Serotec, UK), CD44 (1:9000 dilution and HIER1 for FFPE, 1:5000 dilution, 4% PFA fixation and HIER2 for cryo sections, clone 156-3C11, abcam, UK), CD74 (1:50 dilution and HIER 1 for FFPE, 1:75 dilution, 4% PFA fixation and HIER2 for cryo sections, clone LN2, abcam, UK), Ki67 (1:200 dilution, PFA fixation, clone MIB-1, DAKO, USA). CCR1 (1:50 dilution and HIER1 for FFPE, 4% PFA fixation and HIER1 for cryo sections, clone

MM0061-7B17, abcam, USA), CXCL9 (1:100 dilution and 33% acetone in methanol fixation for cryo sections, clone MM0220-7F11, abcam, UK), CD11b (1:50 dilution and 33% acetone in methanol fixation for cryo sections, clone 2Q902, abcam, UK) and CXCL10 (1:50 dilution and 33% acetone in methanol fixation for cryo sections, clone 6D4, abcam, UK), interferon-alpha2 (1:50 dilution, clone EBI-1, eBioscience) and interferon-gamma (1:00 dilution, clone B27, BioLegend). Rabbit antibodies recognizing human PD-L1 (1:50 dilution and HIER2 for FFPE, 1:150 dilution and 4% PFA fixation for cryo sections, polyclonal, abcam, UK), CCR3 (1:800 dilution, HIER1 and 4% PFA fixation for cryo sections, clone Y31, abcam, UK), CD4 (1:150 dilution and 4% PFA fixation for cryo sections, clone SP35, Zytomed Systems, Germany), CD11b (1:500 dilution and 4% PFA fixation, clone EP1345Y, abcam, UK), CD8 (1:150 dilution and 4% PFA fixation for cryo sections, clone SP16, Zytomed Systems, Germany) and CEACAM5 (1:100 dilution, clone 327, Sino Biological).
Classical H&E and TUNEL staining was performed according to manufacturer's description (In situ cell death detection kit, Roche, Germany) and serial sections were used to quantify dead tumor cells by comparing TUNEL vs. morphological analysis. As the side-by-side comparison of tissue sections confirmed the excellent diagnostic value of morphological analysis as published previously (Duan et al., 2003), morphological analysis was the preferred method for evaluation.

## Western blotting.

Tissue lysates were prepared, protein concentrations were determined and adjusted to 10 µg and separated by sodium dodecyl sulfate polyacrylamide gel electrophoresis (SDS-PAGE) following protein transfer on a polyvinylidene difluoride (PVDF) membrane by semi-dry electroblotting. After an 1 hr blocking step membranes were incubated with the primary antibodies at 4 °C overnight following incubation with the HRP-conjugated secondary antibody for 1 hour according to the manufacturer's protocol. ECL reagent (Pierce ECL Western Blotting Substrate, Thermo Fisher Scientific Inc., Germany) was used to visualize labeled proteins. Antibodies recognizing p38 (polyclonal rabbit, New England Biolabs, Germany) and actin (mouse, clone C4, MP Biomedicals, USA; HRP-anti-mouse IgG, Dianova, Germany) were used as loading controls.

## Flow cytometry.

Surface staining was performed as follows: for each 100 µl FACS buffer 2,5 µl CD3-V450 ( 560365, BD, Germany), 1,25 µl CD4-PerCP-Cy5.5 (560650, BD, Germany) and 2,5 µl CD8-APC-H7 (641400, BD Biosciences, Germany) were used, followed by 20 min incubation on ice (protected from light) and centrifguation. Intracellular staining was then performed by taking up cells into 1% PFA and incubation for 15 min followed by three washing steps with 0.1% Saponin buffer (and centrifugation). Staining of CCL5 was performed as follows: for each 100 µl 0.1% Saponin buffer 5 µl anti-human-RANTES (CCL5)-eFluor660 (AF647, eBioscience, UK) or isotype control mouse IgG2bk-eFluor660 with 1,25 µl (AF647, eBioscience, UK) were used, followed by 15 min incubation at room temperature (protected from light) and two washing steps with 0.1% Saponin buffer. Labeled cells were then subjected to FACS using a BD Biosciences FACS Canto II cytometer (Harvard Stem Cell Institute), gated against negative controls.

To establish the positive control prior to measuring the tumor tissue and to identify lymphocyte populations, healthy donor lymphocytes were treated as outlined above. See **Figure S2E** for an example of a positive control.

## Horizontal matrigel migration models.

Experiments were repeated with extracted T cells from tumor tissues (see above) and showed similar results, although with slower migration speed of T lymphocytes.

## Organotypic functional tumor explant models.

Ex vivo organotypic tissue cultures of primary patient material have the ability to both maintain organ and cellular architecture while also preserving the integrity of the tumor–stroma interaction. As mouse models recapitulating advanced stage metastatic colorectal cancer after multiple treatments are not available, we decided to use direct patient material as „tumor explant models". With the approval of the local ethics committee and after obtaining written consent from the patient, surgical removal of liver metastases of colorectal cancer in advanced stage patients opened the door for retrieval of fresh invasive margin of liver metastases. The material was directly after resection placed in 0.9% NaCl solution, placed on ice and transferred to the laboratory (<30 min total). There it was assessed, cut into (where possible) approximately 5 x 3 x 1 mm blocks and placed into the culture chambers. Medium was added (MEM) and 150 µl DMSO or 150 µl maraviroc (diluted in DMSO 4 nM final concentration). Tissue culture was performed at 37 °C in a 5% CO2 humidified incubator using 1 ml of medium als outlined above. Tissues were cultured in MEM (10xMEM, Gibco, USA) and 1% glutamine (PAA, USA).and treated with the designated inhibitors for 24 to 72 h as indicated. For harvesting tissue blocks were frozen in liquid nitrogen. For reference purposes of each specimen one tissue block was directly frozen and from another block lysates were generated before culture.

In the first step continuity of the preservation of the histology over time and the effects of the media were estimated. Serial blocks from the same samples were treated for 24, 36 or 72h and assessed for their histological resemblance of the directly frozen material (see **Figure S3A**).

As these treated cultures showed high fidelity to the original directly frozen material up to 48h or more the cytokine and chemokine preservation over 48h was assessed. Serum containing media as well as serum-free media were used. The results showed the best fidelity for the simple MEM medium for a time range of 48h (see **Figure S3B**). Media themselves did not contain significant amounts of cytokines (data not shown).

In the next step the fidelity of chemokines and cytokines across the time range (and especially across the first 48 hr) was evaluated. Multiple comparisons of tissue samples from different patients at different time points as well as serial harvesting of cultured adjacent liver indicated the first 48 hr to be the window of opportunity for tissue culture effects (see **Figure S3C**), indicating the time window with a modest trade-off for cytokine stability and a reasonable amount of time for changes in the microenvironment. Experiments with functionally blocking antibodies against CXCL9 and CXCL10 (used at 1µg/ml each) showed reverse effects for the microenvironment as witnessed for CCR5 blockade on the cytokine level (**Figure S4I**). Blocking antibodies used were anti-human CXCL9 (see above), anti-human CXCL10 (rabbit polyclonal, abcam), anti-human CCL5 antibody (goat polyclonal AF-278-SP, RnD, used at 1µg/ml) and anti-human CCR5 antibody (mouse monoclonal [45531] MAB-182-SP, RnD, used at 25µg/ml). Liposomes were used as indicated by previous publications (Claassen et

al., 1990). In addition it needs to be mentioned that all tissue specimens analyzed naturally contain CCL5 in relevant amounts, also if they are marked as "untreated" or control tissue.

## Phase I clinical trial.

We first investigated the clinical impact of maraviroc by performing a clinical trial using the FDA-approved (indication: treatment of HIV infection) CCR5 inhibitor maraviroc as monotherapy for patients with irresectable metastatic colorectal cancer after all standard of care treatments. As maraviroc is metabolized via the liver it was decided in accordance with the regulatory authorities to perform a phase I trial with concomitant biopsies to ascertain CCR5 receptor positivity of tumor cells. In this trial not only the safety of maraviroc standard treatment in patients with extensive liver metastases was evaluated but also the effects of CCR5 blockade on the tissue level. Serial biopsies of the same liver metastasis before and under treatment were performed. Ethics committee approval and further details can also be found at www.clinicaltrials.gov/show/NCT01736813. Eleven of the twelve patients received daily maraviroc 300 mg/bid after being tested for CCR5 receptor positivity in a liver metastasis. One patient was tested but never received maraviroc due to a rapid tumor progression. In all patients the treatment was very well tolerated (see **Table 3**). Most common side effects were mild elevation of liver enzymes, especially in case of tumor progression. No case of postural hypotension was observed. Pre-existing pathological laboratory tests for liver enzymes were present in most of the patients (even up to grade IV) before participation in the trial. No SAE occurred, four instances of grade IV adverse events were recorded. These were however only laboratory value deteriorations in patients that already had grade III levels of these respective laboratory values before treatment. All grade IV events were clinically insignificant (i.e. lab value elevations) and occurred in the course of disease progression. Given the massive pre-trial injury of the liver and the extensive metastatic burden within the liver of these patients, treatment with the CCR5 inhibitor was surprisingly well tolerated. Side effects could be managed (e.g. in the outpatient clinic) and were transient. No dose limiting toxicity was observed.

In addition to the eleven patients directly on the trial, we were allowed to follow-up on three patients that were screening failures due to technical impossibility to biopsy a lesion but then received maraviroc 300 mg/bid as per protocol as individual medical decisions. These patiens had given informed consent and were suitable in their overall status. An amendment for the trial was granted by the ethics committee and the regulatory authorities to include and present data from these three patients also. These three patients form the "extension cohort" because they received maraviroc as per protocol and were followed in our institution. Identically to the patients on trial, these patients were evaluated clinically for safety and followed for one year.

The impact of monotherapy was analyzed with a) standard imaging using magnetic resoncance imaging and as a measure of biological activity b) a second biopsy under treatment. Imaging analyses were evaluated according to Response Evaluation Criteria in Solid Tumors (RECIST) and biopsy evaluation consisted of histological evaluations and dedicated cytokine quantifications. As the experience with clinical trials using immunomodulatory drugs has shown delayed or non-classical responses to these interventions (Wolchok et al., 2009), we also decided to follow these patients for subsequent responses and evaluated the clinical course over one year (imaging analyses as outlined above). The pre-clinical analyses had shown a profound modulation of the immunological microenvironment and we therefore speculated that we might pick up effects of this immunological conditioning in subsequent therapies.

On the trial no patient formally experienced a partial or complete remission. One patient had a mixed response with lung lesions dissapearing but also mild progression in few liver metastases so that this patient missed a classification as partial remission (RECIST -20%).

At the time of protcol development for this trial regorafenib was still investigated and only after ethics committee and federal authorities approval regorafenib was FDA approved and available also in the EU. As our protocol aimed at treating patients having received all standard of care medication it was foreseeable that also patients with pretreatment of regorafenib would want to participate in the MARACON trial. To account for this pre-treatment a separate statictical analysis of the patients with regorafenib pre-treatment was set but showed no specific negative effect on survival effects (data not shown).

The median progression-free survival (PFS) for the 11 patients was 1.15 months (95% confidence interval 0.66 months to infinity), for the extension cohort 1.55 months (1.35, 1.55 and 3.29 months). Median overall survival (OS) was 5.06 months for the core cohort (95% confidence interval 3.06 months to infinity) and 6.94 months for the extension cohort (6.91, 6.94, 16.08 months). Combined cohorts showed a median overall survival of 6.18 months (95% confidence interval 4.34 to 14.07 months). It needs to be mentioned that progression-free survival analyses in this trial are difficult to interpret as the requested weekly safety monitoring (in contrast to the commonly used bi-weekly or longer visits) of patients (including laboratory testing) yielded early detection of suspected tumor progression and therefore this approach is likely to skew the actual progression rate towards an earlier timepoint.
Patients from the MARACON trial were heavily pretreated, which is also reflected in the patient characteristics. Using data from the CORRECT trial (phase-III trial of regorafenib) some aspects are immediately apparent (CORRECT trial vs. MARACON): the fraction of patients with 4 or more previous therapies is higher (47 vs. 63.64%), the fraction of patients with rapid progression under therapies is higher (less than 18 months, 18 vs 36.36%) and the BRAF mutation positive patients are more frequent (4.0 vs 9.1%) (Grothey et al., 2013). In the MARACON core cohort 18% of patients had pretreatment with regorafenib and in the extension cohort 66.67% were already pretreated with this drug. On the MARACON trial LDH levels were generally above upper limit of normal (ULN) and therefore indicate a patient group with an especially poor prognosis. Together, treatment with maraviroc showed a very favorable safety profile and first evidence for therapeutic effects in patients with advanced metastatic colorectal cancer after all standard of care treatments.

In addition to the observations on the overall survival, also effects on the response to subsequent other therapies were seen. From the 11 patients of the core cohort, five went on to receive chemotherapy after participation in the trial. Patients were allowed to receive maraviroc in combination with chemotherapy as the biopsies from the trial had shown anti-tumoral effects on a tissue level and interferon production is associated with a better response to chemotherapy. All RECIST evaluations were repeated independently two months later and confirmed the observed responses (with the exception of the patient with stable disease, who rejected to have further imaging studies). Within the core cohort a tumor control rate of 80% was achieved (extension cohort: 66%).

Patient treatment and monitoring processes are outlined as follows. Patients with refractory metastatic (liver and other sites) colorectal cancer after standard of care chemotherapy were enrolled on an open-label, monocentric phase I trial (clinicaltrials.gov NCT01736813). The study protocol and informed consents were approved by the local institutional review boards (IRB) and by regulatory authorities. All patients had measurable disease documented by magnetic resonance imaging (MRI). Patients who had received chemotherapy within the last three weeks before enrollment, had a documented history of autoimmune disorders, significant viral infections (HIV, Hepatitis C etc.) or had other severe medical conditions, especially required treatment with systemic corticosteroids, were excluded. In summary, a patient on the MARACON trial had on average 4.5 previous therapies and already 2.5 metastatic sites affected by tumor metastases. All patients had liver metastases. Patient demographics are shown in Supplemental Table 1 and Tables 1 and 2 in the main manuscript. Patients received 300 mg/bid maraviroc on each study day for sixty days. Maraviroc was purchased from Pfizer.

Assessment of efficacy was based on a) tissue level response as analyzed by serial biopsy of the same lesion before and under therapy and b) tumor response defined by Response Evaluation Criteria in Solid Tumors (RECIST) version 1.0. Disappearance of all known lesions was counted as complete response (CR). A reduction of at least 30% in the sum of the longest diameter (LD) of target lesions was defined as partial response (PR). Progressive disease (PD) was defined as a >20% increase in the sum of LD of the target lesions from the smallest sum LD recorded since starting therapy, or the appearance of one or more new lesions, or unequivocal progression of existing nontarget lesions. For each patient with a PR, a confirmatory scan was obtained at least 30 days later.

Progression-free survival (PFS) is the time from the date of the first active treatment to date of first documentation of progression or death due to any cause; for PFS, patients last known to be alive, on treatment or within 30 days of discontinuation of treatment, and progression-free are censored at the date of the last objective disease assessment that verified lack of disease progression. Overall survival (OS) is the time from the date of the first active treatment to date of death due to any cause. All patients died during follow-up. Two patients died within the time period of observation (30 days) after last intake of maraviroc. These patients had tumor progression with ileus and progressing liver metastases as identified by clinical and pathological analyses (independent of the trial).

## Supplemental References

Castro, F., Dirks, W.G., Fahnrich, S., Hotz-Wagenblatt, A., Pawlita, M., and Schmitt, M. (2013). High-throughput SNP-based authentication of human cell lines. Int J Cancer *132*, 308-314.

Claassen, I., Van Rooijen, N., and Claassen, E. (1990). A new method for removal of mononuclear phagocytes from heterogeneous cell populations in vitro, using the liposome-mediated macrophage 'suicide' technique. J Immunol Methods *134*, 153-161.

Conzelmann, M., Wagner, A.H., Hildebrandt, A., Rodionova, E., Hess, M., Zota, A., Giese, T., Falk, C.S., Ho, A.D., Dreger, P., *et al.* (2010). IFN-gamma activated JAK1 shifts CD40-

induced cytokine profiles in human antigen-presenting cells toward high IL-12p70 and low IL-10 production. Biochem Pharmacol *80*, 2074-2086.
Duan, W.R., Garner, D.S., Williams, S.D., Funckes-Shippy, C.L., Spath, I.S., and Blomme, E.A.G. (2003). Comparison of immunohistochemistry for activated caspase-3 and cleaved cytokeratin 18 with the TUNEL method for quantification of apoptosis in histological sections of PC-3 subcutaneous xenografts. J Pathol *199*, 221-228.
Wolchok, J.D., Hoos, A., O'Day, S., Weber, J.S., Hamid, O., Lebbe, C., Maio, M., Binder, M., Bohnsack, O., Nichol, G., *et al.* (2009). Guidelines for the evaluation of immune therapy activity in solid tumors: immune-related response criteria. Clinical cancer research : an official journal of the American Association for Cancer Research *15*, 7412-7420.